Mixed-Layer Model Solutions of Equilibrium States of Stratocumulus-Topped Boundary Layers.

Jan Melchior van Wessem

Master's Thesis

Supervisor: Dr. Stephan de Roode

Clouds, Climate and Air Quality
Department of Multi-Scale Physics
Faculty of Applied Sciences
Delft University of Technology

2011

Abstract

The influence of clouds on the radiation feedback of the atmosphere is not well understood. To gain more understanding a Mixed-Layer Model (MLM) for the stratocumulus-topped boundary layer is used to study steady-state solutions. For this purpose the three mixed-layer equations for q_t, θ_l and z_i that fully describe the atmospheric boundary layer are provided and are closed with simple though realistic parameterizations for the surface and entrainment fluxes of moisture and heat. It is shown that the entrainment parameterization of Nicholls Turton results in a numerical model and that a second parameterization, that of Moeng, is used to obtain a very simple and less realistic, yet very illustrative analytical model. Both models are conclusively used to analyse the influence of some key atmospheric variables, most notably the free atmosphere conditions and the sea surface temperature (SST).

A complete description of the free atmosphere is setup and with the MLM multiple simulations for different combinations of free atmosphere humidity and temperature are performed. It is shown that both these conditions significantly effect the steady-state solutions for, in particular, the cloud thickness. A dry and warm free atmosphere corresponds with thin clouds and a moist and cool free atmosphere with thick clouds.

Within this investigation the large-scale horizontal advection is introduced. It is shown that while it does not effect the steady-state solutions much it does provide more realistic solutions in which the vertical flux gradients of moisture and heat are represented better, and can therefore be more efficiently used in, for instance, intercomparisons of single column models.

The main scope of the thesis is to research the effect of a climate change on the steady-state solutions. To research this effect the original solutions are perturbed by an increase of the sea surface temperature of 2 degrees. The effect this increase has on the thickness of the cloud layer is studied and it is shown that effectively four regimes can be distinguished: the cloud thickens, the cloud thins, the boundary layer becomes decoupled and the boundary layer is always decoupled. These four regimes will all have a different feedback effect on the climate change as they either positively or negatively influence the radiation balance of the atmosphere. It is however also shown that the way the free atmosphere changes when the SST changes could change these respective scenarios such that only a thickening or a decoupled regime is found.

Contents

Chapter 1

Introduction

1.1. Background

Weather has an enormous influence on how we experience our live on earth. Everybody participates in predicting the weather either just to know if the sun will shine in two hours or to predict weather evolution around the globe for days to come. In both cases numerical weather forecast models are used to serve this purpose and therefore much research is being done to evaluate, improve and validate these models. Within this research it has become, in the recent past, of a quickly increasing importance to study the global climate change. What causes this climate change remains not well understood. To public consensus it is caused by the greenhouse effect; the effect that the temperature on earth rises due to the ever increasing emission of greenhouse gases like carbon dioxide. It could also be that there are other reasons why this temperature increase occurs. Debated is that it can be caused by either a perpetual cycle of global temperature that has been observed during the livespan of the earth or ocean currents like El Nino. Whatever the case the overall trend is clear: there *is* a temperature increase and it can lead to a severe melting of the polar ice caps with its well know consequences.

There is however one thing that is often overlooked and often underestimated and therefore the focus of this Master's thesis: the influence of clouds on this climate change. Clouds have an enormous influence on the radiation balance on earth. Clouds reflect solar radiation back to space while meanwhile they also retain infrared radiation emitted by the surface of the earth. Furthermore they also emit their own longwave radiation. Because there are numerous different clouds and they all possess their own characteristics it is extremely complicated to exactly predict their contribution but also their response to the climate change. Especially this reaction is interesting. The global temperature increase might lead to more clouds as there will be more evaporation of water. Would this indeed be what happens, and this is unclear and surely not the only effect, then this would reflect more solar radiation resulting in a decrease of temperature. On the other hand the increase of temperature leads to an atmosphere that can actually contain more water vapor and cloud formation will be hampered. It seems there is a subtle competition between the different atmospheric reactions to the climate change. The fact that this reaction is distinct for any given cloud, and there are many kinds, and that even the contribution of a single cloud is diffferently predicted by each model results in a big uncertainty as the following figure shows.

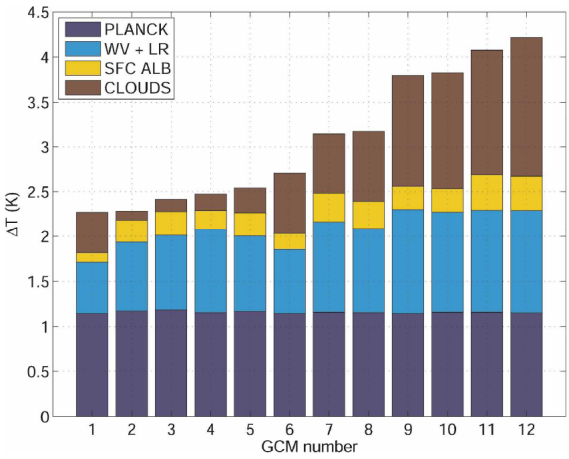

Figure 1.1. Change of temperature ΔT for 12 different climate models due to a sudden increase of carbon dioxide concentration $2 \times CO_2$ resulting in a radiative forcing. Four different effects can be noted: increased planck radiation, more longwave radiation absorption, a different surface albedo and a highly uncertain cloud response.[1]

Figure 1.1 depicts the respective reaction of 12 different climate models to a sudden climate change invoking perturbation (in this case a doubling of CO_2 that effectively leads to the temperature change). It shows that the cloud reaction is significantly different for every model. The reactions due to other parameters like Planck (infrared) radiation, more longwave radiation absorption due to the moister atmosphere and the change in surface albedo, while possibly of a bigger effect, are nevertheless roughly predicted equally by the different models. To improve the certainty and the mutual agreement of the models it is therefore most interesting to improve the understanding of the cloud influence itself.

This research and thesis is focused on one particular cloud: Stratocumulus, the one cloud that is expected to have the biggest influence on the radiation balance. It is a low level cloud (located at about a height of $1km$) and these types of clouds, also Cumulus and Stratus, are the most abundant in the atmosphere. Stratocumulus clouds furthermore have the highest cloud cover of the low level clouds and thus have, area averaged, the biggest reflectivity. This results in the highest interaction with the radiation balance of all the clouds and makes the cloud very interesting to research. Moreover, as stratocumulus clouds cover a big area (sometimes in the order of $10^6 km^2$) and have a simple and homogeneous structure they are relatively easy to study. The following section therefore treats the cloud in some more detail.

1.2. Stratocumulus

Stratocumulus (Sc henceforth) clouds are, as said, one of the three low level clouds. As all clouds are heavily influenced by surface conditions of the earth they are thus very sensitive to climatic changes. In order for Sc to be maintained a sufficient transport of moisture into the atmospheric boundary layer should be present and this causes Sc to mostly exist across the sea or ocean surface. This specifies the research in this thesis on the marine Sc boundary layer. Another ideal prerequisite for Sc to exist is a relatively cool

atmosphere as this lowers the saturation humidity and clouds are formed sooner. Therefore Sc is mostly found across cool ocean currents, for instance along the costs of Peru and California, and moreover it restates the influence the climate change might have.

Sc is also supported by the presence of large scale subsidence in the vicinity of high pressure systems. The subsidence works as a lid that presses down on the boundary layer and enhances low level cloud formation. This is what coincidentally is the case for the Sc areas as found near Peru and California which are located around the so-called horse latitudes. Figure 1.2 shows the so-called Hadley circulation in which this effect is seen.

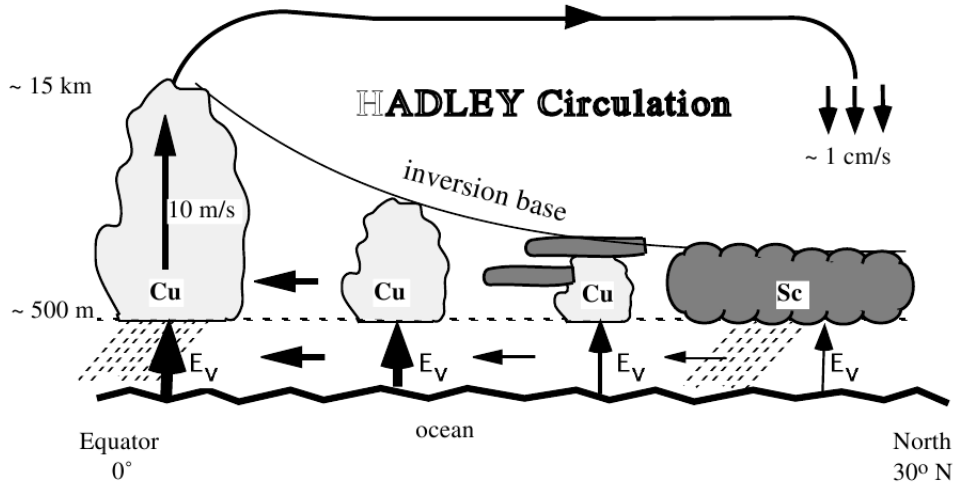

Figure 1.2. A schematic representation of the Hadley Circulation. At the equator evaporation E_v is largest. The rising air caused by the evaporation reaches the free atmosphere and is advected to the subtropics at 30° latitude. As the descending air is relatively much warmer than the underlying boundary layer this determines a very stable stratification of which the intersection is called the inversion base. This stratification encourages Sc formation. Then the trade winds that are opposite to the transport in the top of the atmosphere the advect the Sc towards the equator. Here a transition from Sc into Cu is observed as inversion height and ocean temperature increase. [2]

The figure shows that near the equator, where the insolation is highest, the warm air rises and is transported to the horse latitudes. Here the main descending air motion is present and it is where Sc typically exists. Because the relatively warm free atmosphere (FA) air lies on top of colder and less dense boundary layer (BL) air there is a very stable stratification. The interface that is located here is called the inversion. Meanwhile the BL air that is located here which consists of the Sc is advected back to the equator by the trade winds.

From now on the figure helps explaining the importance of this research. When moving to the equator (to the left in the figure) the sea surface temperature (SST) goes up and together with a decreasing subsidence this gradually increases the inversion base and eventually the advected Sc dissolves and Cumulus clouds (Cu) are formed. This invokes a big change in cloud cover and thus a big effect on the radiation balance. One of the hypotheses of this thesis is therefore that, when for example there is an increase of SST

due to the climate change, this might encourage the Sc transition into Cu and would have a particular positive feedback on the temperature.

Dynamics
The vertical transported moisture that is essential for the formation of Sc is actually due to turbulent eddies. For Sc this turbulence is mainly produced by the longwave radiative cooling of the cloud layer itself. If Sc are sufficiently dense and thick (typically $\approx 100m$) they approximately behave as a blackbody radiator. It is this behaviour that maintains the turbulence, and thus the Sc, in the BL. Within the cloud there is no net cooling as the same radiation that is emitted is also absorbed. At the edges of the cloud this is different. At cloud base there is infrared radiation coming from the surface and the subcloud layer. This results in a slight net warming as the SST is usually higher than the temperature of the cloud base. Meanwhile at cloud top there is, during night, no solar radiation and no heating effect except for a negligible longwave radiation of the air above. Therefore there is a significant net cooling at cloud top. This net cooling forces air parcels higher up in the the cloud to fall which creates most of the turbulence in the Sc Topped Boundary Layer (STBL) (as they mix with the relatively warmer and less dense parcels that have moved from the cloud base upwards due to condensation).

While the turbulent eddies that transport the moisture upwards that is important for the creation of clouds there is a second effect important for this creation. At the top of the STBL some strong enough turbulent eddies can overshoot into the free atmosphere. By falling back into the BL, as they are colder than the FA, they drag warm and dry air with them. This mechanism of mixing FA air with BL air is called entrainment and is assumed to be crucial for a proper understanding of the evolution of the STBL. There are a number of effects this entrainment induces and they are difficult to predict, resulting in the main reason why it is so hard to understand the STBL evolution. The main effect is that the entrainment results in a dissolving of Sc but there are conditions under which the cloud actually thickens. In any case it is assumed that the mixing of the air does moisten the area just above the inversion and causes the inversion to rise and the BL to deepen.[3].

1.3. Equilibrium behaviour and cloud evolution

To gain more insight in the dynamics of Sc clouds and ultimately learn more about their influence on the earth's radiation balance equilibrium states for the STBL are sought. Obtaining these so-called steady-state solutions will provide some knowledge about convergent and longterm behaviour of the BL and especially of the cloud itself. This also becomes relevant when adressing the main theme of this thesis, the effect of a climate change on the Sc clouds. Having a discription for this steady behaviour one could discover what the dominating and eventual effect of the STBL would be when, for instance, the SST is increased by a few degrees. Within this thesis not only this latter effect will be researched but in general everything will revolve around these important equilibrium states.

Eventually these steady-state solutions will give information about whether, given different particular BL conditions, the Sc will on longer time-scales, thicken or thin or that a transition into Cu will occur. To understand this

evolution it is important to characterize the two main parameters controlling the thickness of the cloud: the cloud base height at which the air becomes saturated and the inversion height that determines the top of the turbulent boundary layer. For a change of cloud thickness to occur this would imply that either the cloud base height or the inversion height changes or that the change of one is stronger than the change of the other. This suggests characterizing the different processes resulting in a change of these heights.

First of all, as introduced in the previous section, entrainment will effectively cause the inversion height to increase. This effect is opposed by the large-scale subsidence that presses down on the boundary layer.

The effects on the cloud base height are more diverse and complex. The entrainment of the warm FA air would increase this height as the saturation humidity would increase. Meanwhile the entrainment of the dry FA air also increases this height as a dryer atmosphere obviously reaches saturation later. From the four aforementioned processes could be concluded that the cloud always becomes thinner as the effect on the cloud base is stronger than the effect on the inversion height. There are three more processes though that could, given the right conditions, fully compensate for the thinning of the cloud. Obviously there is the longwave radiative cooling of the cloud layer that effectively cools the cloud layer. More important are the turbulent surface fluxes of moisture and heat that also control the saturation level and effectively enhance the cloud formation.

All in all knowledge of these five processes that control the cloud base and the two processes that control the inversion provides enough information to determine exactly how the Sc evolves. Furthermore, when considering the equilibrium state of the STBL a condition is sought in which these seven processes are exactly in a balance with eachother. Now a climate change implies a disruption of this balance and hints at a new equilibrium condition. Finding these conditions is the topic of this thesis

1.4. Research goal and outline

The goal of this research is to find equilibrium solutions of the Stratocumulus-topped boundary layer. For this purpose a simple Mixed Layer Model (MLM) is used to gain insight in the atmospheric physics that are at work in the boundary layer. Earlier researches, that of Schubert [4], Lilly [5] and Stevens [6], have treated these solutions before. Therefore within this thesis some new understanding is sought by researching the influences of parameters not previously investigated. Most importantly this concerns the influence of the free atmosphere conditions above the boundary layer. Stevens for one has assumed these conditions to be constant and by applying a parameter space of different free atmosphere conditions on the MLM his research can be extended. Another parameter that has in previous researches not yet been implemented in the MLM is the horizontal advection and it is introduced to study its influence. Furthermore an analytical model is constructed to accompany the MLM.

Ultimately these equilibrium solutions will, like in the research of Schubert, be treated for a simulated climate change: an increase of the SST. For a given set of free atmospheric conditions the model will then give information whether the Stratocumulus clouds would thicken, thin or even transition into Cumulus. Conclusively it can then be related to a feedback process: If

more Sc is created a negative feedback possibly compensates for the climate change. If the Sc dissolves or when Cu is formed a positive feedback would actually enhance the climate change and result in an even stronger dissolving of Sc.

This fits right within the worldwide research currently being done: CGILS (CFMIP-GCSS Intercomparison of Large-Eddy and Single-Column Models [7]). This research compares the equilibrium solutions of different Large-Eddy and Single-Column Models which, as figure 1.1 suggests, could differ by a lot. As these models are much more detailed and complex than the MLM, this thesis will hopefully provide some general and illustrative results to back up the CGILS results.

Outline

This thesis is divided into the following parts: First in chapter 2 the theory as necesarry to understand the atmospheric physics at work is treated. Within this chapter most attention will be spent on explaining the numerical mixed layer model as used throughout the entire research. Chapter 3 then discusses the first results: the numerical and analytical steady-state solutions for the different free atmosphere conditions and the intercomparison of the numerical with the analytical model. Chapter 4 then builds on chapter 3 and extends it by treating the influence of a climate change on the steady-state solutions. Finally the general conclusions will be presented followed by recommendations for future research.

Chapter 2

Theory

Before arriving at the main scope of this research it is relevant to have some basic understanding of all the principles at work in atmospheric physics.

This chapter will therefore present the major physics underlying this subject. As many new variables will be introduced first the main thermodynamics will be explained. Conclusively the governing equations as used throughout the thesis will be treated. These equations then result in the Mixed Layer Model, the model that is the basis of the whole research. Finally, in the latter sections, the physics around the research theme will be explained. This includes the steady-state solutions and the parameters of which the influence on these solutions is studied.

2.1. Thermodynamics

All Stratocumulus physics evolves around two important conserved variables: the liquid potential temperature θ_l and the total specific humidity q_t:

$$\theta_l = \theta - \frac{L}{c_p} q_l \tag{2.1}$$

and

$$q_t = q_v + q_l. \tag{2.2}$$

This section will treat the relevant equations to determine these variables: the equations of density, moisture and heat.

To start, as we are interested in the characteristics of the atmosphere one wants to be able to write numerous variables as a function of height. Pressure and temperature relations are therefore very important. First of all the pressure can be expressed by the hydrostatic balance:

$$\frac{\partial p}{\partial z} = -\rho g. \tag{2.3}$$

with p the pressure, ρ the density of air and g the gravitational acceleration.

Secondly we have the universal gas law for an ideal gas (as what the atmosphere can approximately be seen):

$$pV = \nu R T. \tag{2.4}$$

Here V is the volume, ν the number of moles of gas and R the universal gas constant. Rewriting such that the gas law is described in terms of density (and thus mass) gives:

$$p = \rho R_d T. \tag{2.5}$$

Here $R_d = 287.05 Jkg^{-1}K^{-1}$ is the specific gas constant for dry air.

Now the potential temperature θ in terms of T will be introduced. θ can be interpreted as the temperature an air parcel would have if it were displaced isentropically to a height where, for instance, the pressure equals $p_0 = 1000 hPa$. This potential temperature is expressed such:

$$\theta = T\left(\frac{p_o}{p}\right)^{\frac{R_d}{c_p}} = \frac{T}{\Pi}. \tag{2.6}$$

Here p_0 is the pressure at the reference height, R_d the dry air gas constant and c_p the isobaric specific heat. Besides: usually the Exner function $\Pi = \left(\frac{p}{p_0}\right)^{\frac{R_d}{c_p}}$ is used. If (2.6) is differentiated with respect to z an expression for the lapse rate $\frac{\partial\theta}{\partial z}$ is obtained:

$$\frac{\partial\theta}{\partial z} = \frac{\theta}{T}\left(\frac{dT}{dz} - \frac{R_d T}{pc_p}\frac{dp}{dz}\right). \tag{2.7}$$

With the hydrostatic balance assumption $dp/dz = -\rho g$ and the gas law $p = \rho R_d T$ the potential temperature lapse rate is expressed in terms of the dry adiabatic lapse rate $dT/dz = -g/c_p = \gamma_d$:

$$\frac{d\theta}{dz} = \frac{\theta}{T}\left(\frac{dT}{dz} + \frac{g}{c_p}\right). \tag{2.8}$$

From this we can deduce that if the temperature follows the dry adiabatic lapse rate then $\frac{\partial\theta}{\partial z} = 0$ and the potential temperature is constant with height. Due to this characteristic θ proves to be a very convenient variable to work with. However, as the atmosphere in the case of this thesis contains clouds, the potential temperature will not be constant with height anymore because in the cloud layer there is latent heat release due to condensation of vapor. To compensate for this change finally the conserved variable θ_l (Eq. (2.1)) is introduced , which will again be constant with height for the entire cloudy boundary layer:

$$\theta_l = \theta - \frac{L}{c_p} q_l$$

Here L is the latent heat of evaporation of water. The added term in this equation corrects for θ by latent heat release.

To arrive at the other conserved variable to describe the cloudy boundary layer the total specific humidity is presented. It can be expressed in terms of the water content in the vapor and liquid phases as in Eq. (2.2):

$$q_t = q_v + q_l.$$

The specific humidity is usually expressed in units $\frac{g\ of\ liquid\ water/vapor}{kg\ air+liquid\ water/vapor}$. This presence of water in air has as a consequence that the gas law, eq. (2.5), needs some corrections. This is caused mostly by the fact that the density of an air parcel containing water vapor is different from the density of an air parcel containing liquid water. Therefore the gas constant R_m has to be introduced. R_m is the specific gas constant for a gaseous mixture of both moist and dry air: $R_m = (1 - q_v - q_l)R_d + q_v R_v$ with $R_v = 461.5 Jkg^{-1}K^{-1}$. It nevertheless proves to be convenient to still work with R_d as then, apart

from the dry gas constant substitution, the gas law remains unchanged if also a virtual potential temperature T_v is introduced. The corrected gas law appears:

$$p = \rho R_m T = \rho \left[1 - q_v - q_l)R_d + q_v R_v\right] T = \rho R_d T_v. \tag{2.9}$$

Here T_v can be used in the same manner as T but represents the temperature a dry air parcel would have if its pressure and temperature were equal to those of wet air. The derivation of T_v can be found in [8] and reads:

$$T_v = (1 + (1 - \frac{1}{\epsilon})q_t - q_l)T. \tag{2.10}$$

Here $\epsilon = R_d/R_v \approx 0.622$. Analogously to (2.6) the virtual potential temperature is defined as:

$$\theta_v = \frac{T_v}{\Pi}. \tag{2.11}$$

The relevance of this virtual temperature can be understood as follows. If p, T_v and ρ are split into a mean and a fluctuating part (Reynolds averaging[1]) and inserted into the gas law, eq.(2.5), the following expression is obtained:

$$\bar{p} + p' = (\bar{\rho}\overline{T_v} + \rho'\overline{T_v} + \overline{\rho}T_v' + \rho' T_v')R_d. \tag{2.12}$$

If this equation is divided by $\overline{p}$ and if the last term on the rhs which consists of a product of two fluctuations is neglected the following equation results:

$$1 + \frac{p'}{\overline{p}} = \frac{\overline{\rho}\overline{T_v}R_d}{\overline{p}} + \frac{\rho'\overline{T_v}R_d}{\overline{p}} + \frac{\overline{\rho}T_v'R_d}{\overline{p}}. \tag{2.13}$$

As the pressure fluctuations with respect to the average pressure are very small $\frac{p'}{\overline{p}}$ can be neglected. Furthermore the first term in the rhs is equal to 1 and the following relation between T_v and ρ results:

$$\frac{T_v'}{\overline{T_v}} = -\frac{\rho'}{\overline{\rho}} \tag{2.14}$$

Substituting the potential temperature:

$$\frac{\theta_v'}{\theta_0} = -\frac{\rho'}{\rho_0}. \tag{2.15}$$

This relation is very important. Buoyancy determines the vertical motion in the atmosphere and the density fluctuations are a measure for this motion. The density is however very hard to measure while the temperature is not. This relation therefore explains that also by the aid of the virtual temperature differences the buoyancy can be determined.

All in all the variables mentioned above, p, θ_l and q_t, can be used to entirely determine the state of the atmosphere.

A final quantity that is useful is the liquid water path LWP (or often just called W). This quantity gives insight in the size of clouds and interactions with clouds and therefore proves to be useful in this thesis. It is simply defined as the vertical integral of liquid water:

$$LWP = \rho \int_0^{z_{top}} q_l dz. \tag{2.16}$$

[1] Reynolds averaging is a technique suited for turbulence analysis. More careful explanations of this and the rest of the derivation are found in [9].

2.2. Turbulent fluxes

At the end of the previous paragraph the importance of the virtual temperature in relation to the buoyancy was emphasized. This buoyancy is very important as it can be used to describe the turbulent eddies that transport the heat and moisture throughout the boundary layer and are thus essential for cloud formation. To understand this importance the turbulent kinetic energy (TKE) equation is introduced:

$$TKE = \frac{1}{2}(\overline{u'^2} + \overline{v'^2} + \overline{w'^2}). \tag{2.17}$$

Neglecting the horizontal terms the vertical velocity variance $\overline{w'^2}$ is a direct measure for the TKE in the boundary layer. Now the importance of the buoyancy becomes clear by introducing the prognostic equation for $\overline{w'^2}$

$$\frac{\partial \overline{w'^2}}{\partial t} = 2\frac{g}{\theta_0}\overline{w'\theta'_v} - 2\overline{w'\frac{\partial \pi'}{\partial z}} - \frac{\partial \overline{w'^3}}{\partial z} - \epsilon \tag{2.18}$$

in which the first term on the rhs is the only term that is positive and produces TKE in the vertical direction. This term represents the buoyancy production term and it is called the buoyancy flux. In order to calculate this term the link of θ_l and q_t with θ_v is explained. They can then be used to arrive at the turbulent buoyancy flux $\overline{w'\theta_v}$.

To arrive there first equation (2.1) is substituted in equation (2.11) and an expression for θ_v in terms of θ_l, q_t and q_l is obtained:

$$\theta_v = (1 + \epsilon_I q_t - \frac{q_l}{\epsilon})(\theta_l + \frac{L}{c_p}q_l) \tag{2.19}$$

Secondly the assumption that $q_t = q_s + q_l$ (q_s is the saturation humidity) is used and all variables are split in an averaged part and a fluctuating part. Thirdly the entire resulting equation is multiplied by the vertical velocity fluctuation w' and finally Reynolds averaged.

$$\overline{w'\theta'_v} = (\epsilon_I \overline{w'q'_s} - \overline{w'q'_l})\left(\overline{\theta_l} + \frac{L}{c_p}\overline{q_l}\right) + (1 + \epsilon_I \overline{q_s} - \overline{q_l})\left(\overline{w'\theta'_l} + \frac{L}{c_p}\overline{w'q'_l}\right) \tag{2.20}$$

Here third order moments have been neglected and in the case for the air below the cloud, where the air is not saturated and $q_s = q_t$, the above equation is easily written down in terms of two coefficients and the vertical fluxes of θ_l' and q'_t :

$$\overline{w'\theta'_v} = A_d\overline{w'\theta'_l} + B_d\overline{w'q'_t} \text{ for } q_t \leq q_s. \tag{2.21}$$

$A_d \approx 1.01$ and $B_d \approx 180$ are the dry coefficients. For the saturated case more complex coefficients are used but in the end a similar expression is obtained:

$$\overline{w'\theta'_v} = A_w\overline{w'\theta'_l} + B_w\overline{w'q'_t} \text{ for } q_t > q_s. \tag{2.22}$$

With wet coefficients $A_w \approx 0.5$ and $B_w \approx 1000$.

As can be seen the important buoyancy flux can be determined by knowledge of the total humidity and the liquid potential temperature fluxes, similar to the determination of the virtual temperature.

2.2.1. Decoupling

Another reason why the buoyancy flux is so relevant is the process of decoupling, in this thesis known as the transition from Sc to Cu: a process that seperates the cloud layer from the subcloud layer when subcloud turbulent eddies are prevented to reach the cloud layer. The buoyancy flux is very important in this process as it is a measure of how effective the boundary layer is vertically mixed. In order to address the magnitude of decoupling a buoyancy flux criterion has been developed by Turton and Nicholls [10]: the buoyancy integral ratio (BIR). It was suggested out of the suspicion that a negative buoyancy flux in the subcloud layer will lead to decoupling. Looking at the TKE equation (Eq. 2.18) one can understand that a negative buoyancy flux will destroy the TKE and mixing in the boundary layer will be hampered. The ratio is calculated as such:

$$BIR = \frac{-\int_{z<z_b} \overline{w'\theta'_v} dz \quad \text{if} \quad \overline{w'\theta_v}<0}{\int_{other\ z} \overline{w'\theta'_v} dz}.$$

If the ratio is sufficiently positive, BIR > 0.15, it means that subcloud thermals can not reach or have trouble reaching the cloud layer, turbulence will die out and Sc will eventually break up. To explain this effect one notes equation (2.21). In order to have a negative subcloud buoyancy flux the dominant term in this equation for the subcloud flux, $\overline{w'\theta'_l}$ ($A_d\overline{w'\theta'_l} \gg B_d\overline{w'q'_t}$), should become negative. Using the inversion flux it can be used to relate decoupling to the term that most efficiently maintains the turbulence in the STBL: the radiative cooling. If the entrainment flux, that causes warming of the STBL, is stronger than the radiative cooling turbulence in the subcloud layer is destroyed and the STBL becomes decoupled. This relation does not hold for the cloud layer itself as there is liquid water present in the cloud causing extra condensation warming and evaporative cooling (included in the wet and dry coefficients A and B). There can thus be a situation in which the cloud layer is turbulent while the subcloud layer is not. This in turn causes the surface fluxes not to be able to reach the cloud layer and eventually the Sc would dissolve (and one assumes that Cu is created).

Besides this physical explanation there is a second reason to elaborate on this effect: the MLM as used in this research is based on the assumption that the BL is well mixed. The negative buoyancy flux implies that this is not the case as the subcloud and cloud layer are decoupled and heat and moisture fluxes will not reach the cloud layer sufficiently enough to keep the BL well mixed. This means that for the region where the STBL is decoupled the MLM is not valid anymore and results should be treated carefully [11].

2.3. Governing equations and conserved variables

The conserved variables θ_l and q_t prove to be very useful in calculations as the atmospheric system can be described solely by this set of variables. For this description a general conservation equation exists. It expresses the variation of a conserved variable in a given volume with time in terms of the difference of the flux at the edges. To account for internal influences the equation also inhibits a source/sink term. As inside a given volume/area the variable is conserved (constant) these are the only contributions to its variation.

With $\psi \in \{q_t, \theta_l\}$ the conserved variable the equation reads:

$$\frac{\partial \psi}{\partial t} + \frac{\partial \psi u_j}{\partial x_j} = S_\psi. \tag{2.23}$$

This equation is written down in tensor notation in which the subscript j denotes the cartesian coordinates $(x_1, x_2, x_3) = (x, y, z)$. For the velocity u_j the index j denotes the direction.

Using traditional Reynolds decomposition to include the contributions of turbulence and writing the equation out the general tendency equation used in this thesis results:

$$\frac{\partial \overline{\psi}}{\partial t} = -\frac{\partial \overline{u'\psi'}}{\partial x} - \frac{\partial \overline{v'\psi'}}{\partial y} - \frac{\partial \overline{w'\psi'}}{\partial z} - \overline{u}\frac{\partial \overline{\psi}}{\partial x} - \overline{v}\frac{\partial \overline{\psi}}{\partial y} - \overline{w}\frac{\partial \overline{\psi}}{\partial z} + S_\psi \tag{2.24}$$

Here the first three terms on the rhs resemble the turbulent fluxes of ψ. The following three terms denote the advection terms. The last term is the source term and it represents the contribution of precipitation and radiation.

2.4. Mixed-Layer Model

In order to gain more understanding of Sc formation and evolution a Mixed Layer Model (MLM) has been set up. It proves to be a very simple model that consists of just three equations and with which many BL characteristics can be explained. For this model equation (2.24) is used and in this section it will be used to arrive at the three MLM equations. First of all some of the assumptions that result in the model are explained.

In a Stratocumulus topped boundary layer (STBL) conserved variables are by approximation constant with height. This means that the vertical gradient of $\bar{\psi}$ drops out of equation (2.24). Furthermore the assumption of horizontal homogeneity in both the turbulent fluxes and gradients of ψ is used, usually valid in Sc fields. This causes the horizontal gradients to drop out. This leaves the simplified tendency equation:

$$\frac{\partial \overline{\psi}}{\partial t} = -\frac{\partial \overline{w'\psi'}}{\partial z} + S_\psi \tag{2.25}$$

This equation is integrated over the boundary layer height z_i using the mixed layer assumptions that the conserved variable is constant across the layer and is in quasi-steady state. This results in (for convenience using ψ_{ml}):

$$z_i \frac{\partial \psi_{ml}}{\partial t} = -(\overline{w'\psi'|_{z_i}} - \overline{w'\psi'|_0}) + \int_0^{z_i} S_\psi dz. \tag{2.26}$$

Here $\overline{w'\psi'}|_{z_i}$ and $\overline{w'\psi'}|_0$ are the fluxes at respectively the top and the surface of the layer. This equation states that the evolution of ψ_{ml} can be solely determined by knowledge of the flux at the surface, the flux at the top of the boundary layer and a source term. The determination of all terms in equation (2.26) will one by one be described:

Inversion height z_i
The tendency equation for z_i is

$$\frac{dz_i}{dt} = \overline{w} + w_e. \tag{2.27}$$

Above equation shows that the height of the boundary layer z_i is controlled, in the case of a STBL, by two phenomena. First there is the subsidence pushing down on the boundary layer. This subsidence $\overline{w}$ is a function of height and reads:

$$\overline{w} = -Dz. \tag{2.28}$$

Here D is the divergence (assumed to be constant with height) and it can be deduced from the continuity equation for incompressible flow $\frac{\partial \bar{u}}{\partial x} + \frac{\partial \bar{v}}{\partial y} + \frac{\partial \overline{w}}{\partial z} = 0$. The vertical gradient is determined by the gradients in the x and y direction: $\frac{\partial \overline{w}}{\partial z} = -(\frac{\partial \overline{u}}{\partial x} + \frac{\partial \overline{v}}{\partial y}) = -D$.

The second phenomenon is the entrainment w_e. This entrainment is what is hardest to determine in most (STBL) atmospheric studies. For variables like this one parameterizations exist that directly or through iteration calculate the variable. The different w_e-parameterizations will be discussed later on. For now it suffices to say that the entrainment causes the inversion height to grow. The subsidence opposes this growth and together they determine the inversion height.

Inversion flux $\overline{w'\psi'}|_{z_i}$
Around the cloud top air from the inversion layer is mixed with cloudy boundary layer air. It is clear that the magnitude of this mixing is controlled by the size of the inversion jump and the magnitude of the entrainment. This influence is summarized in the following parameterization for the flux:

$$\overline{w'\psi'}|_{z_i} = -w_e \Delta\psi \tag{2.29}$$

where $\Delta\psi = \psi_{fa} - \psi_{ml}$ is the jump where the subscript fa denotes the free atmosphere value.

Surface flux $\overline{w'\psi'|_0}$
The surface flux has also been parameterized:

$$\overline{w'\psi'}|_0 = C_D|\vec{U}|\left(\psi_0 - \psi_{ml}\right). \tag{2.30}$$

Here $C_D = 0.001\left(1 + 0.07|\vec{U}|\right)$ is an exchange coefficient, $|\vec{U}|$ is the absolute velocity relative to the surface and ψ_0 is the value directly at the surface (and is determined by the SST).

Source/sink terms S_ψ
The source term usually represents precipitation, shortwave (solar) radiation and longwave radiation. In this thesis precipitation and solar radiation are neglected[2] and the source term for the longwave radiation remains:

$$\int_0^{z_i} S^R_{\theta_l} dz = -\frac{1}{c_p \rho_0} dF_L. \tag{2.31}$$

Here dF_L is the difference between the radiation contribution at the top and at the surface of the BL (in Sc the contribution is actually located in the

[2] An explanation of the implementation of precipitation and shortwave radiation can nevertheless be found in [10].

upper $50m$ of the BL) and thus represents a resulting constant radiation. From aircraft measurements it has been concluded that the net longwave radiation is usually in the order of $70Wm^{-2}$. The solar radiation can if needed also be included in this term by treating it as a constant correction to the source term. Then the net radiation is in the order of $dF_{rad} = 30Wm^{-2}$.

The model equations

With all the terms in equation (2.26) now adressed for the model equations for q_t and θ_l result. Together with equation (2.27) they are a proper tool to determine the characteristics of the mixed layer. For q_t:

$$z_i \frac{dq_{t,ml}}{dt} = C_D|\vec{U}|(q_{t,0} - q_{t,ml}) + w_e \Delta q_t. \tag{2.32}$$

and for θ_l :

$$z_i \frac{d\theta_{l,ml}}{dt} = C_D|\vec{U}|(\theta_{l,0} - \theta_{l,ml}) + w_e \Delta\theta_l - \frac{1}{c_p \rho_0} dF_L; \tag{2.33}$$

These equations will be used during this thesis and typical profiles for $q_{t,ml}$ and $\theta_{l,ml}$ are show in figure 2.1. The main complexity in finding a full solution for these equations lies in the entrainment parameterization and will be handled in section 2.4.3.

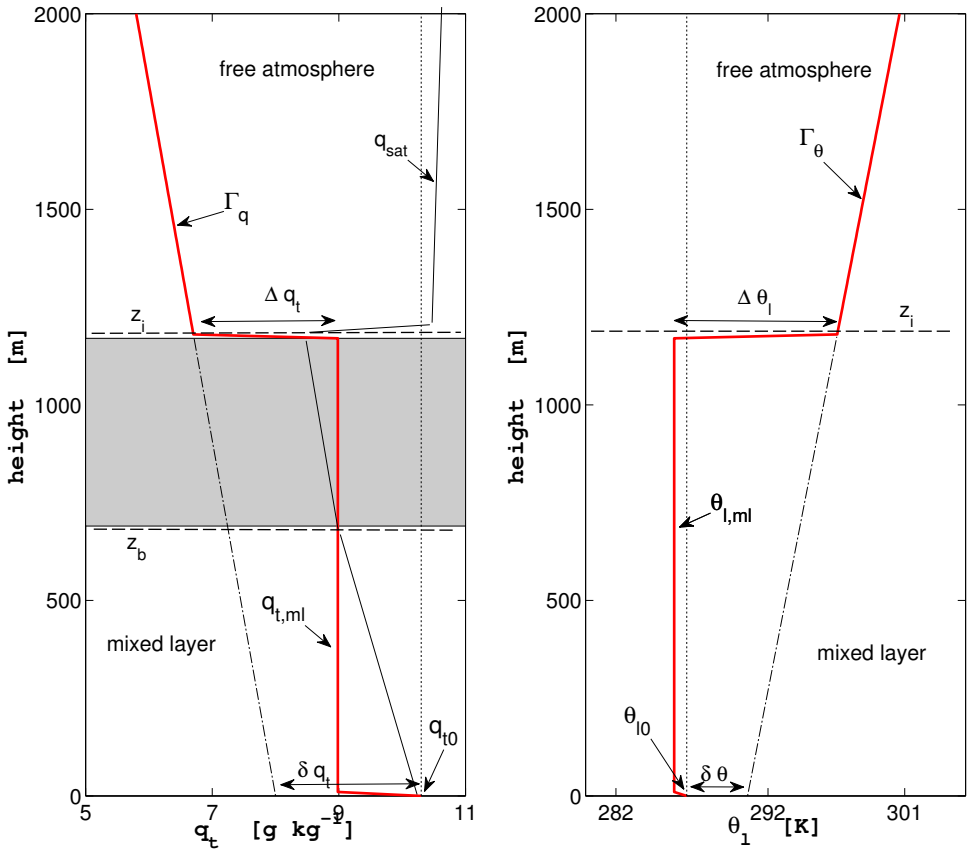

Figure 2.1. Typical profiles for q_t and θ_l in a STBL. First it is shown that the cloud base is located where $q_{t,ml} = q_{sat}$ and the cloud is shaded in gray. The plot further shows the way the free atmosphere profile is set up by both $\delta\psi$ and ψ_0: The lapse rate is extrapolated from a surface value equal to $\psi_0 + \delta\psi$. In this case $\psi_{ref} = \psi_0$, but this is just an arbitrary choice. Would the inversion height be higher it would imply a new free atmosphere condition.

2.4.1. Steady-state

Investigating steady-state solutions of the STBL is the main emphasis of this research. Therefore the cause and effect of the STBL reaching a steady-state will be elaborated on in this section. Using the fact that in steady-state $\frac{\partial}{\partial t} = 0$ equation (2.25) can be written:

$$-\frac{\partial \overline{w'\psi'}}{\partial z} + S_\psi = 0. \tag{2.34}$$

This equation says that to reach steady-state there should be a balance of the turbulent flux gradient and the source term. Using the mixed layer equations (2.32) and (2.33) derived in the previous section the steady-state equations result:

$$C_d|\vec{U}|\left(q_{t,0} - q_{t,ml}\right) = -w_e \Delta q_t \tag{2.35}$$

and

$$C_d|\vec{U}|\left(\theta - \theta_{l,ml}\right) = -w_e \Delta\theta_l + \frac{dF_L}{\rho_0 c_p}. \tag{2.36}$$

If the relationship $\Delta\psi = \psi_{fa} - \psi_{ml}$ is used one can solve for ψ_{ml} to gain some simple equations as a means of achieving some first qualitative insight:

$$q_{t,ml} = \frac{C_d|\vec{U}|q_{t,0} + w_e q_{t,fa}}{C_d|\vec{U}| + w_e} = q_{t,0} + \frac{w_e\left(q_{t,fa} - q_{t,0}\right)}{C_d|\vec{U}| + w_e} \quad \text{and} \tag{2.37}$$

$$\theta_{l,ml} = \frac{C_d|\vec{U}|\theta_{l,0} + w_e\theta_{l,fa} - dF_L/\rho_0 c_p}{C_d|\vec{U}| + w_e} = \theta_{l,0} + \frac{w_e\theta_{l,fa} - \theta_{l,0} - dF_L/\rho_0 c_p}{C_d|\vec{U}| + w_e}. \tag{2.38}$$

From these equations the influence of absolute wind velocity $|\vec{U}|$ and entrainment w_e are found. For large $|\vec{U}|$ the mixed layer converges to the surface value while for large w_e the inversion dominates and the model converges to the free atmosphere value. Furthermore a large longwave radiative cooling dF_L indeed shows cooling of the whole layer. Rewritten a bit, as in the most rhs equations, they show the combined effect of the free atmosphere and the surface.

Even more illustrative is the steady-state equation for z_i. Writing equation (2.27) in steady-state gives a very direct counterbalance between subsidence and entrainment:

$$w_e = Dz_i. \tag{2.39}$$

The equation effectively shows that steady-state is reached by reaching a balance between the entrainment that tends to heighten the boundary layer and the subsidence that pushes it down. It too shows, together with the previous equations, the importance of w_e as it appears in all three equations.

2.4.2. Free atmosphere conditions

Also very important in this thesis are the free atmosphere conditions. The implementation of these conditions in climate models, named $q_{t,fa}$ and $\theta_{l,fa}$, tends to be significantly different given the research. To be able to

completely describe the free atmosphere condition so its influence can be studied they are in this research defined the following way:

$$q_{t,fa} = q_{ref} + \delta q_t + \Gamma_q z \quad \text{for} \quad z > z_i, \tag{2.40}$$

and

$$\theta_{l,fa} = \theta_{ref} + \delta\theta_l + \Gamma_\theta z \quad \text{for} \quad z > z_i. \tag{2.41}$$

The first term on the rhs denotes an arbitrary value that is connected to the surface value of humidity and temperature. It is typically equal to the surface values $q_{t,0}$ and $\theta_{l,0}$ but in some of the experiments performed in this thesis it proves to be important that it can be varied independently. On top of this reference value an extra contribution $\delta q_t < 0$ or $\delta\theta_l > 0$ is added. It represents a direct measure for the condition of the free atmosphere and is directly related to the inversion jump.

Finally a contribution due to a vertical lapse rate Γ in the free atmosphere is considered; its usage together with the surface conditions is shown in figure 2.1.

To understand where the lapse rates originate from equation (2.24) is used and evaluated within the free atmosphere. As there is no turbulence here (outside of the BL) the turbulence terms drop out and the equation can be written:

$$\frac{\partial \psi_{fa}}{\partial t} = -\overline{w}\Gamma_\psi - \vec{U}\frac{\partial \psi_{fa}}{\partial x_h} + S_\psi. \tag{2.42}$$

Here are seen the tendency contributions due to the lapse rate and a horizontal advection term (subscript h stands for all horizontal directions). The source term as before only turns up in the temperature equation in the form of radiative cooling. With this equation in mind the functioning of the lapse rates can be explained. It shows that, when positive, it can have a moistening/warming effect (subsidence $\overline{w} < 0$). In the Hadley circulation for instance it is a assumed that a horizontal homogeneity is found in the free atmosphere making the advection term drop out and finally simplifying above equation to:

$$\frac{\partial q_{t,fa}}{\partial t} = -\overline{w}\Gamma_q \quad \text{and} \tag{2.43}$$

$$\frac{\partial \theta_{l,fa}}{\partial t} = -\overline{w}\Gamma_\theta - \frac{1}{\rho c_p}\frac{\partial F}{\partial z}. \tag{2.44}$$

As this thesis mainly treats steady-state solutions it is assumed that in the free atmosphere there too is steady-state. This information can provide some understanding in what values the lapse rates can have. For $q_{t,fa}$ the lapse rate Γ_q has to be typically equal to zero; there is no term that can balance a finite value for this term, unless there is horizontal advection which is only realistic in some cases. For $\theta_{l,fa}$ on the other hand there is a balancing term in the form of the radiation contribution and a finite temperature lapse rate does seem to be more realistic. In practise this is indeed what is found. For researching purposes though both lapse rates will be considered. Together with δq_t and $\delta\theta$ they form an interesting set of conditions that will be investigated thoroughly.

2.4.3. Entrainment

The entrainment of environmental air into the boundary layer, that ultimately causes the boundary layer to grow, depends on many boundary layer parameters and is therefore one of the more complex quantities in boundary layer research. Therefore parameterizations are created that use the boundary layer parameters to calculate the entrainment.

One of the most simple parameterizations is Moeng's (CM) [12]:

$$w_e = \frac{0.2\overline{w'\theta'_l}|_0 + \frac{dF_L}{\rho_0 c_p}\left[2.5 - 2exp(-b_m\sqrt{LWP})\right]}{\Delta\theta_l}. \tag{2.45}$$

With $b_m = 0.03$. It gives w_e as a function of the surface flux $\overline{w'\theta'_l}|_0$, the longwave radiative cooling of the cloud and the inversion jump $\Delta\theta_l$. As it only takes into account the temperature jump it is a very limited parameterization. Nevertheless it will prove to be of use in this thesis, particularly in finding analytical solutions.

A better and thus more complicated parametrization is the one of Nicholls and Turton (NT) [13].

It starts with a convective BL (CBL) parameterization:

$$\frac{w_e}{w^*} = \frac{A}{Ri_{w^*}}, \tag{2.46}$$

where $A \approx 0.2$.

$$w^{*3} = \frac{2.5g}{\theta_0}\int_0^{z_i} \overline{w'\theta'_v}dz \tag{2.47}$$

is the convective velocity scale as a function of the bouyancy flux across the boundary layer. The Richardson number is linked to this scale and reads:

$$Ri_{w^*} = \frac{gz_i}{\theta_0}\frac{\Delta\theta_v}{w^{*2}}. \tag{2.48}$$

This, when written out, gives

$$w_e = \frac{A}{gz_i}\frac{\theta_0}{\Delta\theta_v}w^{*3}, \tag{2.49}$$

an implicit relation as w_e depends on w^*. To solve for w^* the integral in (2.47) is split into two terms:

$$\Theta \equiv \frac{1}{z_i}\int_0^{z_i} \overline{w'\theta'_v}dz = \Theta_{NE} + \Theta_E. \tag{2.50}$$

Here Θ_{NE} includes all processes not related to the entrainment and Θ_{NE} represents the entrainment contribution to the buoyancy flux. Further discription of this calculation is found in [13] resulting in the following expression for w_e :

$$w_e = \frac{2.5A\Theta_{NE}}{\Delta\theta_{v,NT} + 2.5A(f_{z,cb}\Delta\theta_{v,dry} + f_{z,cld}\Delta\theta_{v,sat})}, \tag{2.51}$$

in which $f_{z,cb} = z_b/z_i$ and $f_{z,cld} = 1 - f_{z,cb}$. They denote the relative contributions of both the subcloud and the cloud layer to the total virtual potential temperature jump $\Delta\theta_v$. Here both jumps are determined by the dry and wet coefficients as in Eqs. (2.21) and (2.22): $\Delta\theta_{v,dry} = A_d\Delta\theta_l + B_d\Delta q_t$ and $\Delta\theta_{v,sat} = A_w\Delta\theta_l + B_w\Delta q_t$. This therefore shows why this paramaterization

is more complete than that of Moeng: it takes into account the humidity jump.

The last thing to note is that this formula is the case for the clear boundary layer. In a STBL $\Delta\theta_v$ is different as extra evaporation and longwave cooling due to the mixing of boundary layer and environmental air plays a crucial role. For NT $\Delta\theta_v$ can therefore be redefined as

$$\Delta\theta_{v,NT} = \frac{\Delta\theta_v}{1 + a_2(1 - \Delta m/\Delta\theta_v)}. \tag{2.52}$$

Here $a_2 \approx 30$, a new constant, and $\Delta m = 2\int_0^1 \Delta\theta_v(\chi)d\chi$ a value denoting the evaporation enhancement due to the different mixtures.

The difference between these two most used parametrizations lies mostly in the fact that CM does not depend on the humidity inversion jump and only on the θ_l-jump. NT on the other hand uses the buoyancy jump which, as can be seen in equation (2.11) and figure 2.2 , depends on both $\Delta\theta_l$ and Δq_t.

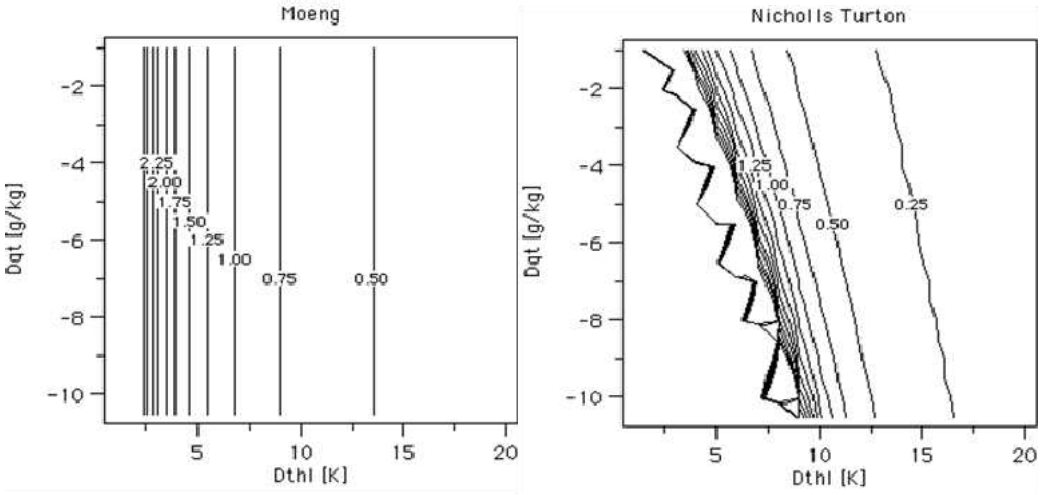

Figure 2.2. The entrainment in cms^{-1} as a function of the inversion jumps $\Delta\theta_l$ and Δq_t for the parameterization of Moeng (left) and that of Nicholls and Turton (right). Main difference is the dependence on Δq_t and the asymptotic behaviour of NT.[13]

2.4.4. Horizontal advection

In the equations derived in section 2.4 it is assumed that the BL is horizontally homogeneous $\frac{\partial\overline{\psi}}{\partial x_h} = 0$. It does prove to be useful and more realistic to include this term in the tendency equations. The third and second to last terms in equation 2.24 resembles the large-scale mean horizontal advection term:

$$\overline{u}\frac{\partial\psi}{\partial x} + \overline{v}\frac{\partial\psi}{\partial y} = U\frac{\partial\psi}{\partial x} \tag{2.53}$$

where it is assumed that U is in the direction of x. Adding the term to equations (2.33) and (2.32) and following the steps used in section 2.4 the new tendency equations for $\psi \in \{q_t, \theta_l\}$ result:

$$\frac{d\theta_{l,ml}}{dt} = \frac{C_D|\vec{U}|(\theta_{l,0} - \theta_{l,ml}) + w_e\Delta\theta_l}{z_i} - \frac{\frac{1}{c_p\rho_0}dF_L}{z_i} - U\frac{\partial\theta_l}{\partial x} \tag{2.54}$$

and

$$\frac{dq_{t,ml}}{dt} = \frac{C_D|\vec{U}|(q_{t,0} - q_{t,ml}) + w_e\Delta q_t}{z_i} - U\frac{\partial q_t}{\partial x}. \tag{2.55}$$

The advection term on the rhs of both equations can still be implemented in a few different ways. This research uses a pre-set advection magnitude related to the SST-gradient which gives a direct relation for both the humidity and the temperature horizontal gradient: $\frac{\partial q_t}{\partial x} \approx \frac{\partial q_{sat}(SST,p_0)}{\partial x}$ and $\frac{\partial\theta_l}{\partial x} \approx \frac{\partial SST}{\partial x}$. Values for this gradient can be gotten from the Hadley circulation (or other realistic cases in which a SST-gradient is present) and is $\frac{\partial SST}{\partial x} \approx 5 \cdot 10^{-3} Km^{-1}$.

Influence on turbulent fluxes in steady-state
Using the tendency equation (Eq.(2.25)) with the horizontal advection included in the source term :

$$\frac{\partial q_t}{\partial t} = -\frac{\partial\overline{w'q_t'}}{\partial z} - U\frac{\partial q_t}{\partial x}, \tag{2.56}$$

and

$$\frac{\partial\theta_l}{\partial t} = -\frac{\partial\overline{w'\theta_l'}}{\partial z} - \frac{1}{c_p\rho_0}\frac{\partial F}{\partial z} - U\frac{\partial\theta_l}{\partial x} \tag{2.57}$$

it can be explained that in steady-state these equations make for some interesting behaviour: as explained in section 2.4.1 the flux gradient in the boundary layer will be zero when horizontal advection is absent: $\frac{\partial\overline{w'q_t'}}{\partial z} = 0$ and $\frac{\partial(\overline{w'\theta_l'} + dF_L/\rho_0 c_p)}{\partial z} = 0$. Here the total heat flux $\overline{w'\theta_l'} + dF_L/\rho_0 c_p$ is considered.

Now by introducing the advection term the gradient will be nonzero and equal to the magnitude of the advection:

$$\frac{\partial\overline{w'q_t'}}{\partial z} = -U\frac{\partial q_t}{\partial x} \tag{2.58}$$

and

$$\frac{\partial(\overline{w'\theta_l'} + F/\rho_0 c_p)}{\partial z} = -U\frac{\partial\theta_l}{\partial x}. \tag{2.59}$$

This effect can be seen in figure 2.3 where some typical flux profiles are shown.. While without advection the flux profile is constant with height, when advection is included the profiles attain a vertical gradient equal to $U\frac{\partial\psi}{\partial x}$. By using the q_t- and θ_l-flux profiles the buoyancy flux profile can then be constructed. This profile can then be used to gain some understanding in the influence of horizontal advection on decoupling and how the inclusion of the horizontal advection affects the validity of the MLM.

It is interesting to note, due to the simplified nature of the MLM, one can analytically calculate the buoyancy flux profile from the knowledge of

the surface fluxes and the magnitude of horizontal advection. To do so the starting point is Equation (2.21), evaluated at $z \leqq z_b$:

$$\overline{w'\theta'_v} = A_d\overline{w'\theta'_l} + B_d\overline{w'q'_t} \quad \text{for} \quad q_t \leq q_s. \tag{2.60}$$

If the advection term is constant so will be the gradient in the respective fluxes. Therefore the surface flux can be extrapolated to obtain the flux at height $z \leqq z_b$ from equations (2.58) and (2.59) as follows:

$$\overline{w'q'_t}|_z = \overline{w'q'_t}|_0 - U\frac{\partial q_t}{\partial x}z \tag{2.61}$$

and

$$\overline{w'\theta'_l}|_z = \overline{w'\theta'_l}|_0 - U\frac{\partial \theta_l}{\partial x}z \tag{2.62}$$

This equation can easily be evaluated and a final expression for the buoyancy flux is obtained:

$$\overline{w'\theta'_v}|_z = A_d\left(\overline{w'\theta'_l}|_0 - U\frac{\partial \theta_l}{\partial x}z\right) + B_d\left(\overline{w'q'_t}|_0 - U\frac{\partial q_t}{\partial x}z\right). \tag{2.63}$$

The same can be done for the region $z > z_b$ by using the wet coefficients A_w and B_w.

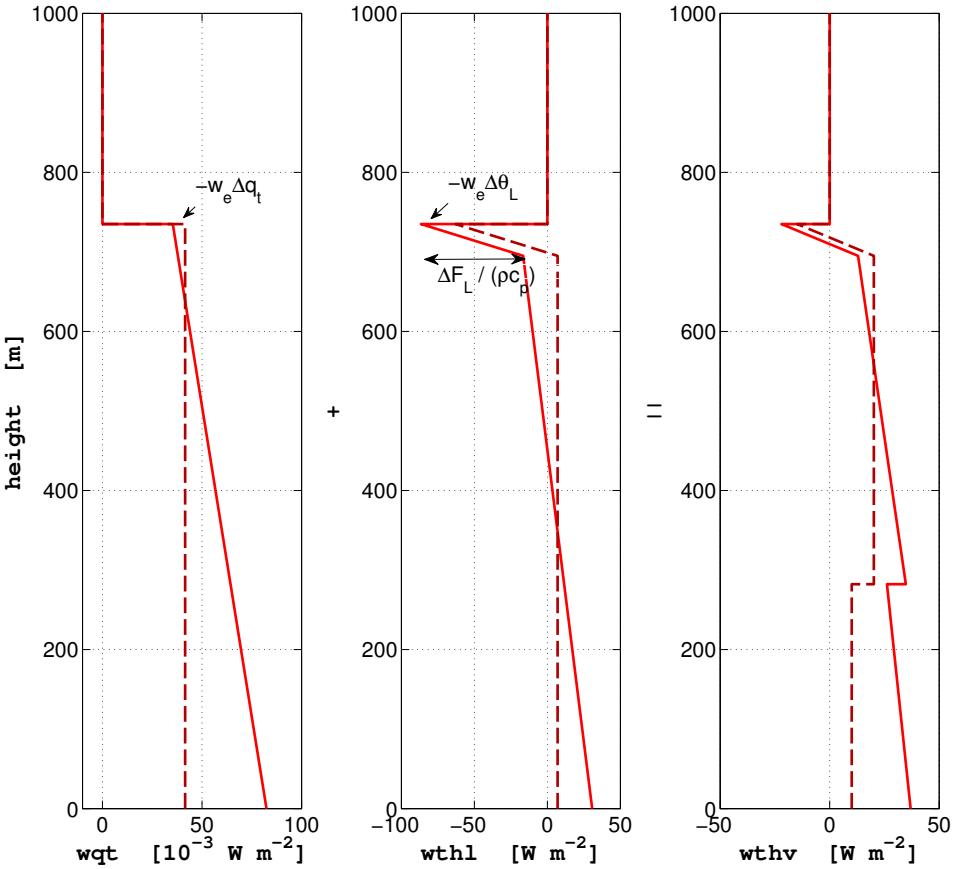

Figure 2.3. Typical steady-state moisture, potential temperature and buoyancy fluxes for a situation with (solid line) and without (dashed) horizontal advection. With respective wet and dry coefficients the buoyancy flux can be constructed from the moisture and heat flux. The difference in the surface fluxes of both profiles is caused by the drying and cooling effect of the advection and will be treated in more detail in section 3.3.

2.4.5. Determination of extra parameters

While most relevant quantities can be determined with the model equations there are still some important quantities to find that are less straightforward to calculate. First it is important that the cloud base level z_b can be specified . The cloud base level is the location at which the liquid water specific humidity q_l is no longer equal to zero, starting at the surface. It is therefore needed to find the point where $q_t = q_{sat}$. This can be done either numerically or analytically. Numerically it is very easy to find this point by intersection like is done in figure 2.1. It does prove to be useful and illustrative to explain the less direct analytical method of determining z_b.

z_b is not straightforward to calculate as it depends on q_{sat} and this value depends on the Clausius-Clapeyron equation. To simplify this equation Stevens [14] has approximated it by linearizing the logarithm of q_{sat} about the surface temperature. The saturation humidity q_{sat} at temperature T then reads

$$q_{sat}(T) = q_{sat}(SST) \cdot exp\left[\frac{L_v}{R_v SST^2}\{T - SST\}\right] \tag{2.64}$$

and when plotted:

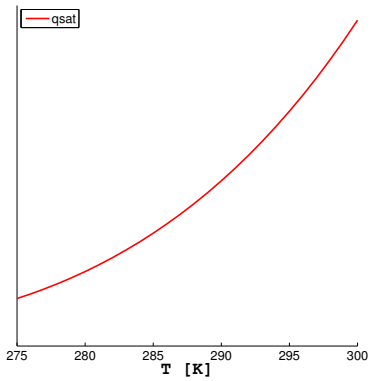

Figure 2.4. Behaviour of $q_{sat}(T_0) = q_{t,0}$ for increasing (sea surface) temperature.

As cloud base is defined as the height at which $q_{t,ml} = q_{sat}$ this equality has to be solved. To do so only an expression for T in terms of z is needed. This is done by noting that in the subcloud layer an air parcel follows the dry adiabatic lapse rate $\gamma_d = -g/c_p$ (the temperature T and thus q_{sat} drop for increasing height). T as a function of height for the mixed layer is then $T(z) = SST + (\theta_{l,ml} - \theta_{l,0}) + \gamma_d z$ (the middle term denotes a small surface jump). Substituted in equation (2.64), evaluated at $z = z_b$ and realizing that $q_{sat}(SST) = q_{t,0}$ the equality as stated above reduces to

$$q_{t,ml} = q_{t,0} exp\left[\frac{L_v}{R_v SST^2}\gamma_d z_b\right]. \tag{2.65}$$

Solved for z_b :

$$z_b = -\frac{R_v SST^2}{L_v \gamma_d} ln(\frac{q_{t,ml}}{q_{t,0}}). \tag{2.66}$$

The cloud base height is thus a function of $q_{t,ml}$ and SST and can now also be used to calculate the liquid water path LWP. For Sc it is as follows [8]:

$$LWP = \frac{1}{2}\rho_{air}\Gamma_{q_l}(z_i - z_b)^2 \tag{2.67}$$

in units $[kg/m^2]$ where $\Gamma_{q_l} \approx 2 \cdot 10^{-6} kg kg^{-1} m^{-1}$ is the liquid water lapse rate (this lapse rate can obviously also be used to calculate the q_l-profile itself).

Chapter 3

Numerical and analytical analysis

This chapter will treat the general steady-state solutions of the MLM. This is done by spanning a range of free atmosphere conditions which eventually results in solutions of a broad and realistic range of STBL parameters.

The research is divided into three parts. First a numerical investigation of the steady-state solutions is provided based on the parameterization of Nicholls Turton. In the second part a similar analysis is done of analytical solutions, based on the Moeng paramaterization, and some of the results are compared. In the last part the influence of boundary layer parameters on the solutions is discussed. Within this discussion horizontal advection is included in the MLM as to research its effect and also to be able to use it for some analyses in chapter 4.

As introduced in equations (2.40) and (2.41) for a given $q_{t,0}$ and $\theta_{l,0}$ (both directly defined by the SST) there are four possible free atmosphere parameters. This section will therefore provide two cases in which these free atmosphere conditions are spanned as depicted in table 3.1. By investigating these solutions new information about the influence of the (changing) free atmosphere humidity can be found, a parameter that most studies have not included. Furthermore the effect of the stabilizing parameter $\Delta\theta_l$, that is determined by both $\delta\theta$ and Γ_θ, is researched. It proves to be a very important parameter in Sc formation and therefore an extra emphasis will be placed on decoupling and the parameters z_i, z_b and LWP. This emphasis then proves to be of importance for the next chapter in which Sc evolution is researched.

This emphasis will then be a starting point for the next chapter that treats the effect of an increasing SST on the results of these two cases.

Table 3.1. The free atmosphere conditions as used in two cases. In each case two parameters will be spanned and two parameters will be kept constant. Below the other relevant conditions are provided.

case	Γ_q $[gkg^{-1}km^{-1}]$	Γ_θ $[Kkm^{-1}]$	δq_t $[gkg^{-1}]$	$\delta\theta$ $[K]$
1	0	6	$-$[0 10]	[$-$2 15]
2	$-$[0 1]	[2 15]	-2	5

SST	288	K
D	5.0	$\times 10^{-6} s^{-1}$
$\lvert\vec{U}\rvert$	7.0	ms^{-1}
dF_L	70	Wm^{-2}
p_0	1029	hPa

3.1. Numerical steady-state solutions

Starting points for the numerical analysis are the mixed layer equations:

$$z_i \frac{dq_{t,ml}}{dt} = C_D|\vec{U}|(q_{t,0} - q_{t,ml}) + w_e \Delta q_t, \tag{3.1}$$

$$z_i \frac{d\theta_{l,ml}}{dt} = C_D|\vec{U}|(\theta_{l,0} - \theta_{l,ml}) + w_e \Delta\theta_l - dF_L/\rho_0 c_p, \tag{3.2}$$

and

$$\frac{\partial z_i}{\partial t} = w_e + \overline{w} \tag{3.3}$$

This time dependent model is run for the parameters as depicted in table 3.1 until steady-state is reached. The entrainment is calculated by the NT parameterization as introduced in section 2.4.3. Furthermore the inititial conditions for $q_{t,ml}$, $\theta_{l,ml}$ and z_i are arbitrary as any strong imbalance of fluxes will converge to the steady-state values, in any case. This consequently causes the timespan in which the model converges to its steady-state not to be representative of any real timespan and therefore no attention will be paid to the parameter t.

Case 1 $\{\delta q_t; \delta\theta\}$

First of all the two lapse rates will be considered constant: $\Gamma_q = 0$ and $\Gamma_\theta = 6Kkm^{-1}$ while altering the jumps as specified in the table. Γ_q and Γ_θ are chosen as found in the atmosphere .

Figure 3.1 shows that the values of LWP that are shown are indeed typical of Sc (typical is an upper limit of $0.5kgm^{-2}$ when the fact that these values are overestimated due to the vertical well mixedness of the MLM is taken into account). In the upper left corner (low δq_t causing Δq_t approach zero) LWP values have gone much beyond that treshhold and are omitted completely in all plots. The dark gray shading denotes the region where surface buoyancy fluxes are negative, implying a region where decoupling starts and Cu clouds are expected to appear and where the MLM does not hold up. The region with the light gray shading denotes another limit: where the cloud base height goes to zero. For this case (and also for the other case) it deserves to be mentioned that the ranges of $\delta\theta$ and δq_t were chosen such as to result in realistic inversion jumps as seen in the second figure, figure 3.2. For instance jumps as found in the ASTEX investigation of decoupling in the Hadley circulation [15], the researches of Stevens [10, 6, 14] or the STBLs used in the CGILS [7] research show jumps of $\Delta\theta_l \approx 10K$ up to $16K$ and $\Delta q_t \approx -2gkg^{-1}$ up to $-8gkg^{-1}$. These ranges of inversion jumps, where therefore Sc is found, moreover typically lie between the two shaded areas: zero cloud base and decoupled STBL.

Going back to the analysis of the liquid water path: It shows a roughly equal dependency on both δq_t and $\delta\theta$. This can be explained by looking at the plots of z_i and z_b which together determine the cloud thickness and thus the LWP. The inversion height and likewise the entrainment show a dependence as expected: the temperature jump $\Delta\theta_l \propto \delta\theta_l$ effectively controls the boundary layer depth. There is also a clear asymptotic behaviour for decreasing $\Delta\theta_l$; the inversion rises quicker the higher it gets. This is caused

by the entrainment parameterization which shows the same behaviour in figure 2.2. Meanwhile z_b shows a clear dependence on both temperature and humidity as it concerns an equality between q_{sat} and $q_{t,ml}$ where the first is influenced by the temperature and the latter obviously by δq_t. It is interesting to note though that $q_{t,ml}$ also possesses a dependency on $\delta\theta$ due to the direct influence of this parameter on w_e.

Considering the research theme of climate feedback it is interesting to discuss why the STBL decouples for small $\delta\theta$. The decoupling starts when there is a negative buoyancy flux in the subcloud layer. As the horizontal advection term has not yet been included in the model the subcloud flux is everywhere equal to the surface flux (Eq. (2.63)). In this equation, as $A_d\overline{w'\theta_l'} \gg B_d\overline{w'q_t'}$, the heat flux is a measure for the magnitude of decoupling. This can be seen as decoupling occurs for a $\theta_{l,ml} > \theta_{l,0} = 285.7K$. The slight derivation from this line is caused by the remaining dependence on the moisture flux. This is an interesting effect as it implies that processes that result in a warmer mixed layer (and do not influence the surface value) encourage decoupling.

At the same time it seems that the decoupling also occurs as the inversion gets higher (around $z_i > 1100m$), particularly in the region where the asymptotic behaviour gets more apparent. It can be explained by the fact that the higher the BL gets the warmer the air that is entrained, due to Γ_θ. This effectively warms the BL causing the equality $\theta_{l,ml} = \theta_{l,0}$ to be reached. It can also be explained by the fact that the entrainment flux $w_e\Delta\theta_l$ that warms the BL is larger than the radiative cooling $dF_L/\rho c_p$ that creates the turbulence. The fact that w_e rises quickly while $\Delta\theta_l$ decreases slowly for lower $\delta\theta$ says that at some point $w_e\Delta\theta_l > dF_L/\rho c_p$ and there is a negative buoyancy in the subcloud layer.

This influence of the free atmosphere conditions is very clear: The humidity and temperature in the free atmosphere together with the surface condition ψ_0 directly determine ψ_{ml}. This was already seen in equations (2.37) and (2.38) that are quite illustrative for these steady-state solutions but now also seen in the plots for $q_{t,ml}$ and $\theta_{l,ml}$. For $\theta_{l,ml}$ it is surprising to note that for increasing $\delta\theta$ (warmer free atmosphere) the temperature in the ML actually drops. Apparently the warming effect of the term $\Gamma_\theta z_i$ in equation (2.41), caused by the BL growing for decreasing $\delta\theta$, is stronger than the cooling effect of decreasing $\delta\theta$. This also seen in the plots for $\Delta\theta_l$. The decrease of $\Delta\theta_l$ is not identical to the decrease of $\delta\theta$. For Δq_t almost the same can be said. Here δq_t mostly resembles Δq_t , as $\Gamma_q = 0$, but for increasing entrainment the deviation from the line $\Delta q_t = \delta q_t$ becomes larger. These respective behaviours of the inversion jumps prove to be important for the evolution of the STBL and will be referred to in the next chapter.

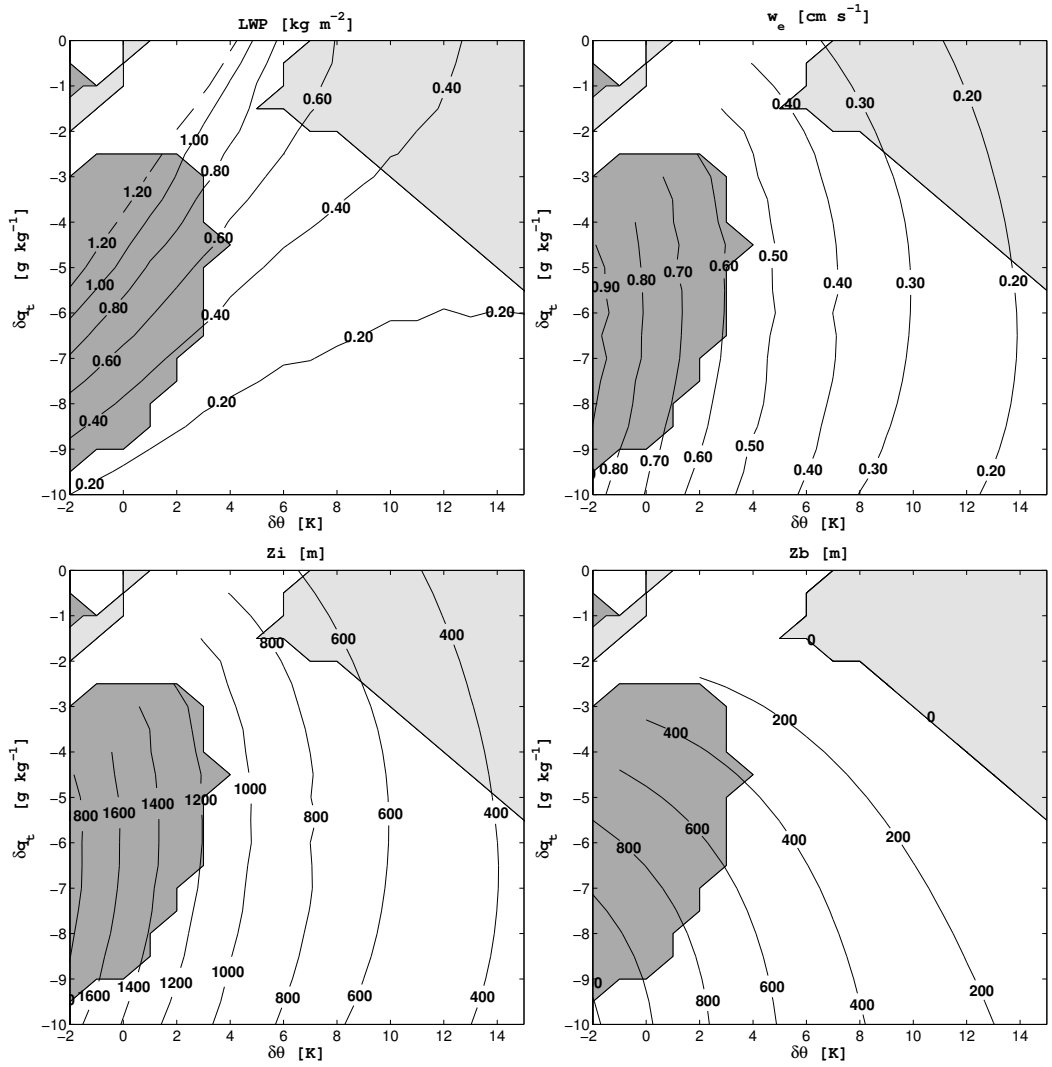

Figure 3.1. Case 1: Steady-state solutions for the first four boundary layer variables: LWP, w_e, z_i and z_b. Shaded in dark gray is the region where the STBL is decoupled. Light gray is where cloud-base is zero. In the upper left corner the conditions become increasingly unrealistic and are for this reason omitted. Boundary conditions are depicted in Table 3.1.

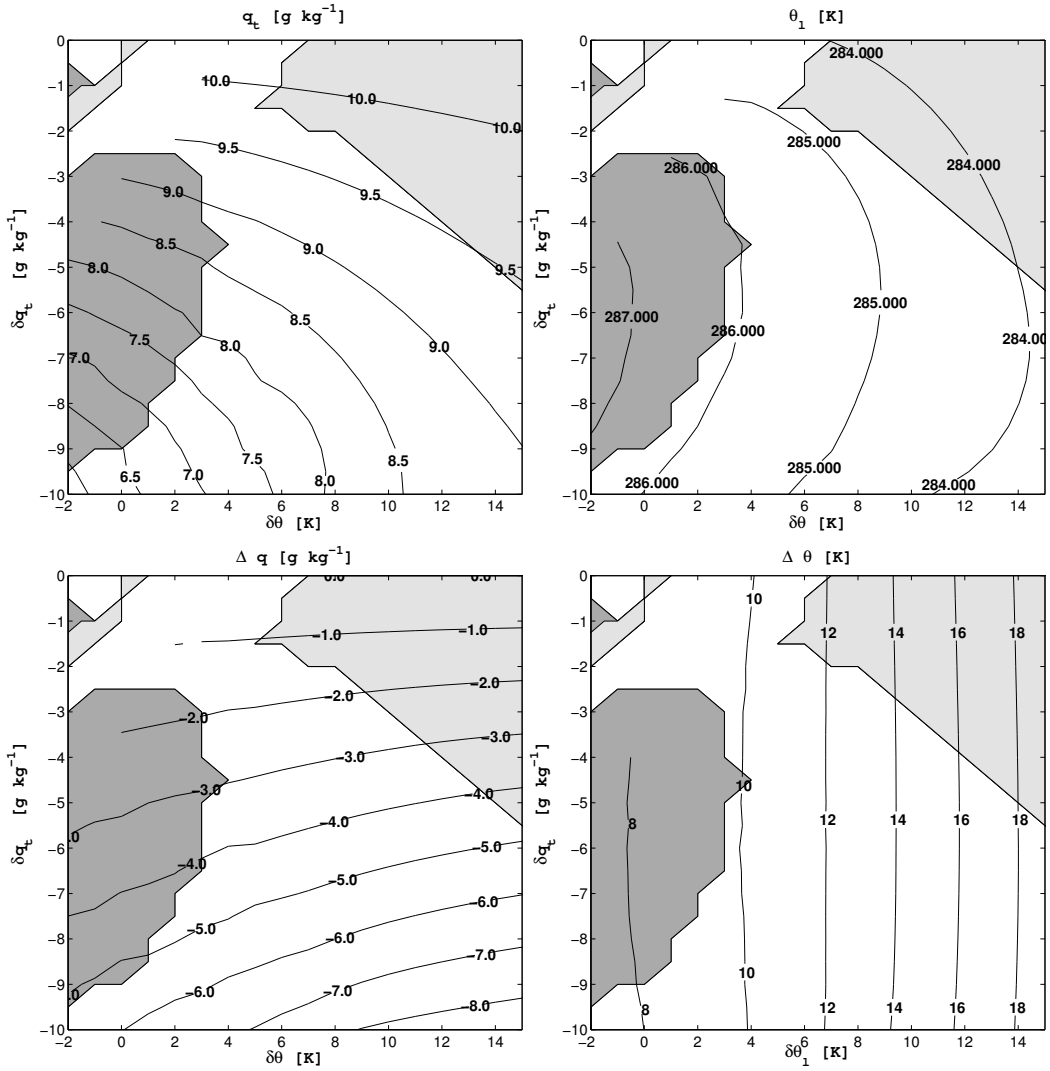

Figure 3.2. Case 1: Steady-state solutions for the final four boundary layer variables: $q_{t,ml}$, $\theta_{l,ml}$, Δq_t and $\Delta\theta_l$. Shaded in dark gray is the region where the STBL is decoupled. Light gray is where cloud-base is zero. In the upper left corner the conditions become increasingly unrealistic and are for this reason omitted. Boundary conditions are depicted in Table 3.1.

Case 2 $\{\Gamma_q; \Gamma_\theta\}$

Now the second case is considered. It is different from case 1 in mainly two things. First now there is a free atmosphere lapse rate for humidity Γ_q. The results in this section therefore will show what its effect will be and how a dependence of $q_{t,fa}$ on height influences the steady-state solutions. Furthermore both Γ_q and Γ_θ will now be altered and thus a stronger dependency of BL parameters on the inversion height z_i is expected. It too does imply that there are now, in a small region, negative values for $q_{t,fa}$ possible (as $\Gamma_q < 0$) . This region at high Γ_q will therefore be shaded in light gray. To make the results comparable to case 1 a similar range of $\Delta\theta_l$ and Δq_t is specified as the region of which the results are shown. These plots will provide the same kind of information about the influence of the free atmosphere conditions on the steady-state solutions of the STBL.

First of all, in the plot for LWP in figure 3.3, a roughly similar behaviour is noticed. The upper left corner that, like before, corresponds with moist and cold free atmosphere conditions enhances cloud formation. Furthermore a slightly stronger dependency on the vertical axis is seen. This is explained by noting that the lapse rate Γ_q effectively causes the free atmosphere condition to be increasingly dryer for increasing inversion height. As z_i still mainly depends on $\Delta\theta_l$ (and in this case on Γ_θ) now Γ_q has created a stronger dependency of $q_{t,ml}$ on $\Delta\theta_l$. This consequently causes Δq_t and z_b to also depend more on $\Delta\theta_l$.

Other than this enhanced influence of $q_{t,fa}$ on the steady-state solutions it remains to be noticed that there is still decoupling for $\theta_{l,ml} \approx \theta_{l,0}$. This region has shifted to the upper left corner and thus implies that, for high Γ_q, turbulence and thus a coupled MLM is enhanced. Apparently the dry free atmosphere causes more evaporative cooling in the cloud and creates more turbulence.

The last effect to note is that, as expected, w_e and thus z_i show an even stronger asymptotic behaviour for increasing values. This is obviously caused by Γ_θ on the horizontal axis instead of $\delta\theta$ and causes much steeper behaviour.

It can be concluded that similar behaviour is noticed compared to case 1 and that providing contourplots based on the lapse rates interesting information is obtained about the influence of the free atmosphere conditions. In both cases the depth of the boundary layer z_i has very big and important influence on the evolution of all other variables. This will prove to be interesting for the next chapter where especially the competition between changes of z_i and z_b will be of importance for determining changes in cloud layer depth but also for the next section where analytical solutions will be sought.

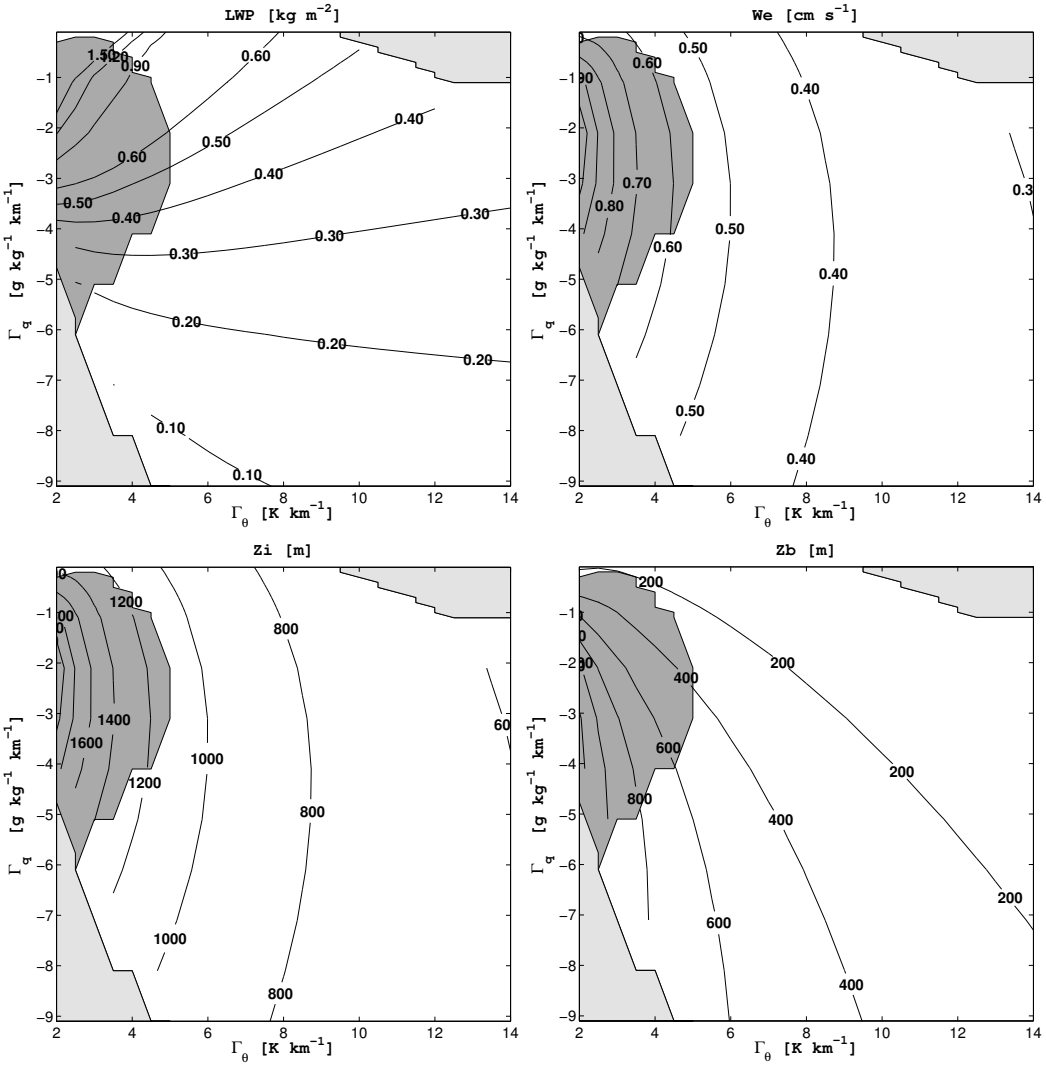

Figure 3.3. Case 2: Steady-state solutions for the first four boundary layer variables: LWP, w_e, z_i and z_b. Shaded in dark gray is the region where the STBL is decoupled. Light gray is where cloud-base is zero. Boundary conditions are depicted in Table 3.1.

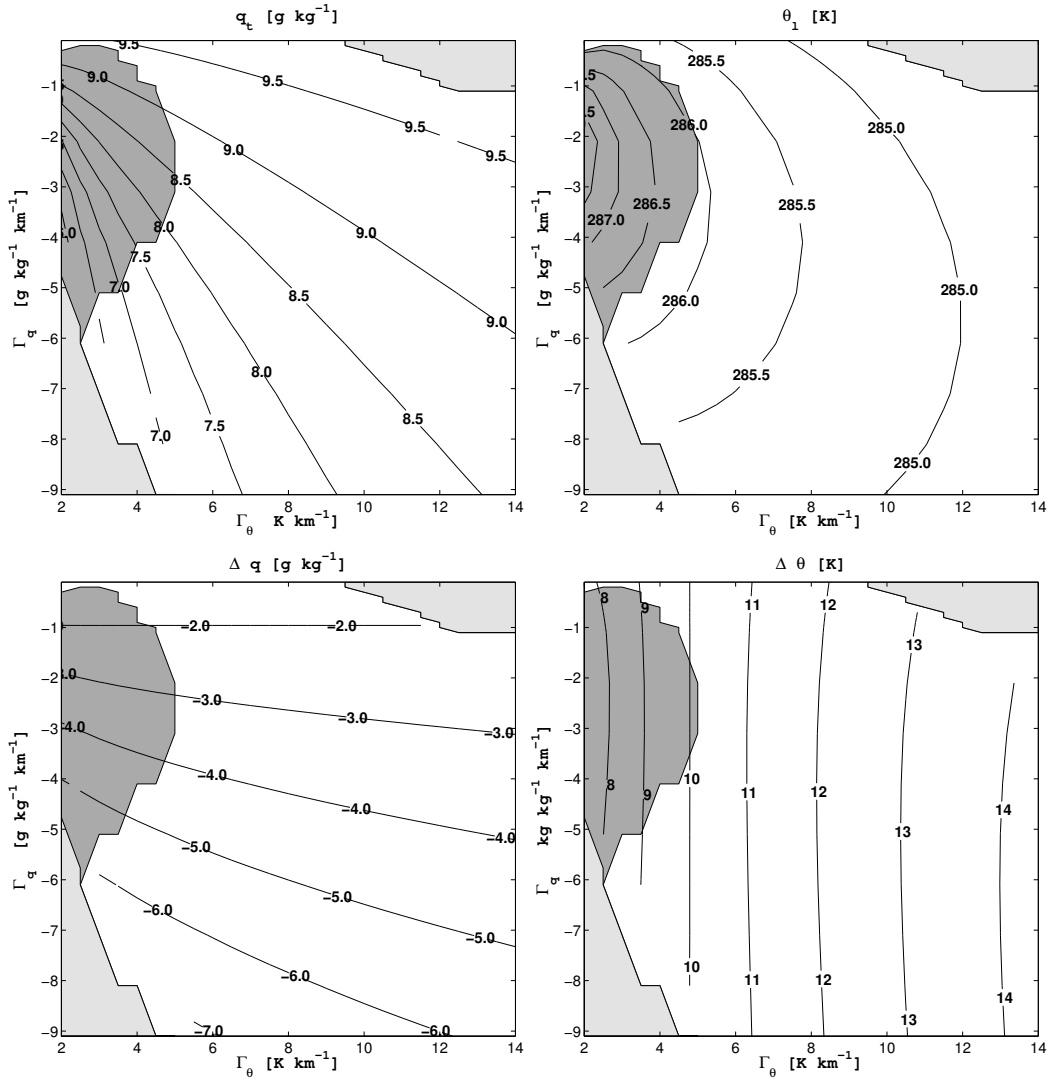

Figure 3.4. Case 2: Steady-state solutions for the final four boundary layer variables: $q_{t,ml}$, $\theta_{l,ml}$, Δq_t and $\Delta\theta_l$. Shaded in dark gray is the region where the STBL is decoupled. Light gray is where cloud-base is zero. Boundary conditions are depicted in Table 3.1.

3.2. Analytical steady-state solutions

Starting points to find the analytical steady-state solutions are the mixed layer equations as in equations (2.37) and (2.38):

$$q_{t,ml} = \frac{C_D|\vec{U}|q_{t,0} + w_e(q_{ref} + \delta q_t + \Gamma_q z_i)}{C_D|\vec{U}| + w_e}, \tag{3.4}$$

$$\theta_{l,ml} = \frac{C_D|\vec{U}|\theta_{l,0} + w_e(\theta_{ref} + \delta\theta + \Gamma_\theta z_i) - F'}{C_D|\vec{U}| + w_e}, \tag{3.5}$$

and

$$w_e = Dz_i. \tag{3.6}$$

Here $F' = dF_L/\rho c_p$. To analytically determine these solutions an expression for w_e is needed. This is done by using the most simple paramaterization, that of Moeng: equation (2.45). It is assumed that in a STBL the radiative cooling dominates, $dF_L/\rho c_p \gg \overline{w'\theta_l'}|_0$. Therefore the entrainment parameterization can be simplified enormously and reads:

$$w_e = \frac{AF'}{\Delta\theta_l}. \tag{3.7}$$

with $A = \frac{w_e\Delta\theta_l}{F'}$ a ratio of the entrainment flux and radiative cooling. This ratio determines whether there is decoupling or not as it represents whether entrainment warming or radiative cooling dominates. It hereby immediately shows the limitation of this simple parameterization, caused by the fact that there is no humidity influence included in the closure. By chosing a value for A it is effectively determined that the boundary layer is decoupled or that the layer is well mixed. There are no circumstances in which the STBL can become decoupled. For Nicholls Turton A changes for different conditions and can reach a value $A > 1$ where the BL is decoupled. For equation (3.7) now $A = 0.7$ is chosen and the BL is not decoupled.

Using this expression that relates the entrainment with the inversion jump $\Delta\theta_l$ there are now four equations and four unknowns ($q_{t,ml}$, $\theta_{l,ml}$, z_i and w_e) and the equilibrium solutions can be calculated. The derivation is located in appendix A and results in analytical expressions for z_i, $\theta_{l,ml}$, $q_{t,ml}$ and using the equations derived in section 2.4.5 also for q_{sat}, z_b and LWP. Given the importance of z_i and the complexity in the other variables only z_i is provided here. The other solutions can be obtained by substituting 3.6 and the equation for z_i (Eq.A.11) in the equations for $q_{t,ml}$ and $\theta_{l,ml}$. This immediately clarifies the importance of z_i: $q_{t,ml}$ and $\theta_{l,ml}$ are just a function of a few constant parameters and mainly the inversion height z_i. It reads:

$$z_i = \frac{1}{2\Gamma_\theta}\left[\frac{(A-1)F'}{C_d|\vec{U}|} - \theta_{ref} + \theta_{l,0} - \delta\theta\right] + \frac{1}{2\Gamma_\theta}\sqrt{\left(\frac{(A-1)F'}{C_d|\vec{U}|} - \theta_{ref} + \theta_{l,0} - \delta\theta\right)^2 + \frac{4AF'\Gamma_\theta}{D}}$$

First of all this equation gives interesting information about z_i as a function of the FA parameters $\delta\theta$ and Γ_θ. Noting that $\theta_{ref} = \theta_{l,0}$ as long as the SST is not altered[1] and just for clarification using $A = 1$ the equation shows a simple dependency on both $\delta\theta$ and Γ_θ :

[1] θ_{ref} is just based on $\theta_{l,0}$. Its influence will only appear in chapter 4 when the SST will be increased and it will either influence the free atmosphere condition or not.

$$z_i = \frac{1}{2\Gamma_\theta}\left(-\delta\theta + \sqrt{\delta\theta^2 + \frac{4F'\Gamma_\theta}{D}}\right). \tag{3.8}$$

It clearly shows the asymptotic behaviour for especially Γ_θ that was apparent from the contourplots in the previous section. It also shows the effects that the other parameters have: increasing divergence D lowers z_i and increasing longwave radiative cooling F' raises z_i. This model seems to be a good tool to find steady-state solutions and especially information about STBL behaviour. To further investigate it similar plots as for the numerical model are now provided in figure 3.5.

First looking at the left panel (resembling case 1) one sees that, except for the slight underprediction, the LWP is predicted well and especially its behaviour towards increasing values in the upper left corner. The dependence of z_i on $\delta\theta$ and not at all on δq_t is also seen, obvious from the simple parameterization which is used. Still the effects of free atmosphere humidity are still visible in the plot for LWP as it comes into the equation due to the dependence of $q_{t,ml}$ on z_i and the dependence of z_b on $q_{t,ml}$ as $LWP \propto (z_i - z_b)^2$.

The fact that LWP is predicted so well encourages using the analytical model further on in this thesis when the influence of an increasing SST will be discussed.

Moving to case 2 it is clear that the LWP is again represented well, albeit less well than for case 1. This is probably caused by the increased influence that Γ_q gives the humidity for increasing inversion height and the fact that the dependence of w_e on humidity is not represented in the simple parameterization.

Overall it can be said that the analytical model provides interesting information, especially about the behaviour of the STBL. Still, due to the fact that the model can not predict decoupling and that the parameterization is incomplete, the numerical model will be used in the rest of this thesis. The analytical model will only nr used to further understand the numerical results.

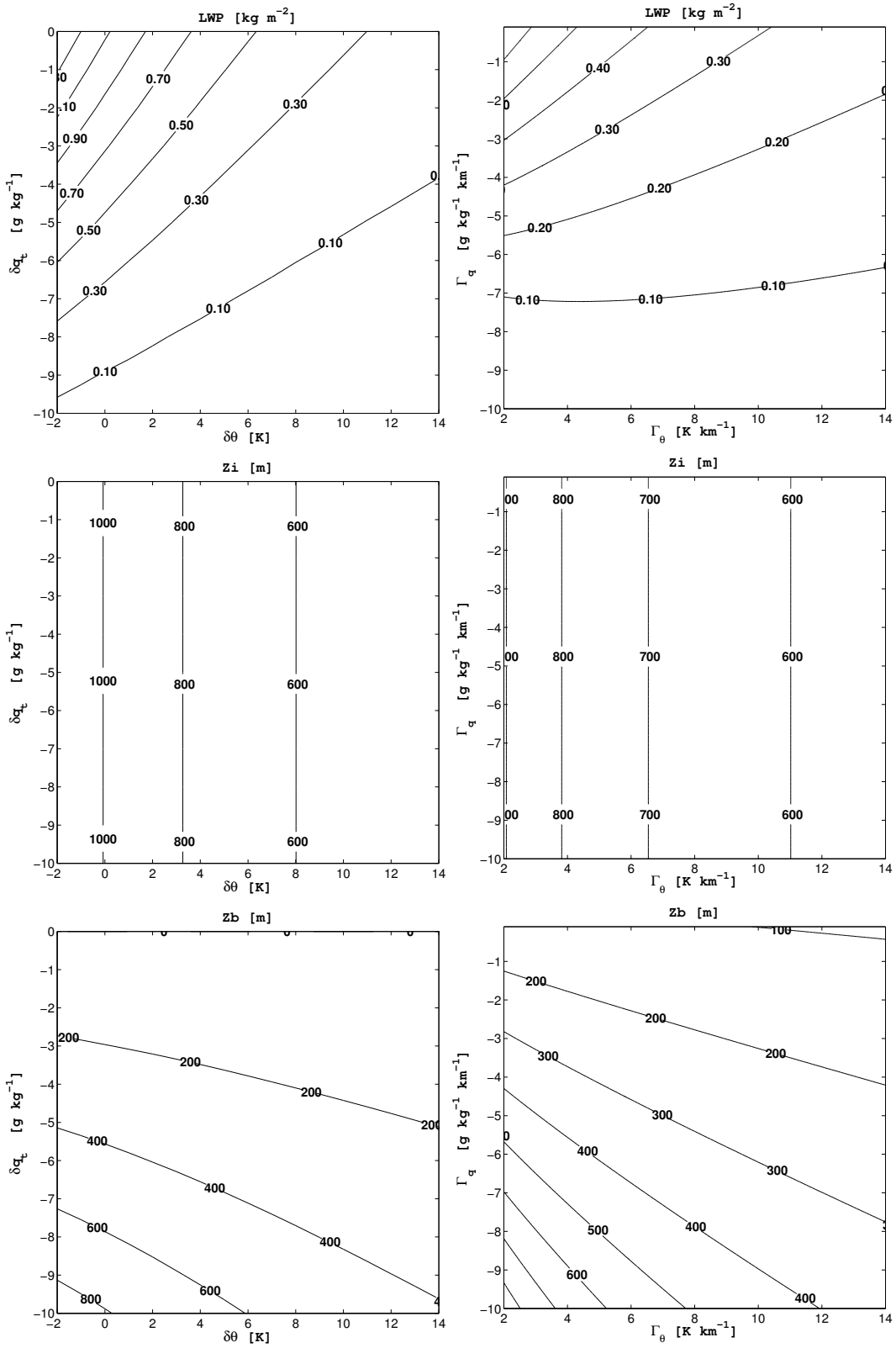

Figure 3.5. Analytical steady-state solutions for LWP, z_i and z_b for cases 1 (left panel) and 2 (right panel). Boundary conditions are depicted in Table 3.1.

3.3. Sensitivity analysis

Not only the free atmosphere conditions influence the steady-state solutions, obviously the other parameters can have interesting effects too. By using the numerical MLM their influences can be simulated easily and therefore this section treats the effects of divergence D, radiative cooling dF_L, velocity $|\vec{U}|$ and horizontal advection $\vec{U}\frac{\partial \psi}{\partial x}$. Especially the latter horizontal advection is interesting to research as its implication will make the model more realistic and useable in the investigations of chapter 4. Besides these parameters also the influence of the SST is addressed and by that means contourplots of LWP for the four forcing terms versus the SST are provided. Here the reference values q_{ref} and θ_{ref} equal to $q_{t,0}$ and $\theta_{l,0}$ at $SST = 288K$ will be used. The fixed value of dF_L has been changed to $dF_{rad} = 30Wm^{-2}$ as to represent a daily averaged radiative cooling as it is the value the next chapter will work with.

Table 3.2. Investigated variables and the range in which they are varied for section 3.3. Free atmosphere conditions are as the fixed values given in Table 3.1.

variable	fixed	range	
SST	288	$[288, 294]$	K
D	5	$[3, 11]$	$\times 10^{-6} s^{-1}$
dF_{rad}	30	$[10, 100]$	Wm^{-2}
$\|\vec{U}\|$	7	$[4, 14]$	ms^{-1}
$\frac{\partial SST}{\partial x}$	0	5.0	$\times 10^{-3} Kkm^{-1}$

3.3.1. Divergence and SST

The divergence is altered from the values as depicted in table 3.2. Figure 3.6 first shows the influence of the SST. Higher sea surface temperature results in an eventual decoupling of the boundary layer. Furthermore, until this decoupling is reached, an increasing LWP is observed. This behaviour proves to be more complicated than this figure shows at first sight, which is caused by the combined effect of all the different parameters. This behaviour will be discussed in more detail in the next chapter. For now the influence of the divergence will be adressed and it is clear: a higher divergence presses down on the boundary layer and LWP is typically smaller in this range. Apparent is the changing gradient in this direction: it means the cloud thickens less for increasing SST as the divergence becomes higher. Overall it can be concluded that D has a big influence on Sc formation as was also obvious from equation A.11.

It is also noted that this plot can nicely be compared to the divergence versus SST steady-state analysis as performed by Stevens in [6]. He has shown that the LWP is very sensitive to the divergence and that it slightly increases towards higher SST. There are still some differences, especially in the magnitude of LWP, that are caused by his different implementation of the free atmosphere (he approximately uses $\delta q_t \approx -3.5 gkg^{-1}$) and a different a_2 for the NT-parameterization. In any case it does confirm the behaviour as found with the MLM.

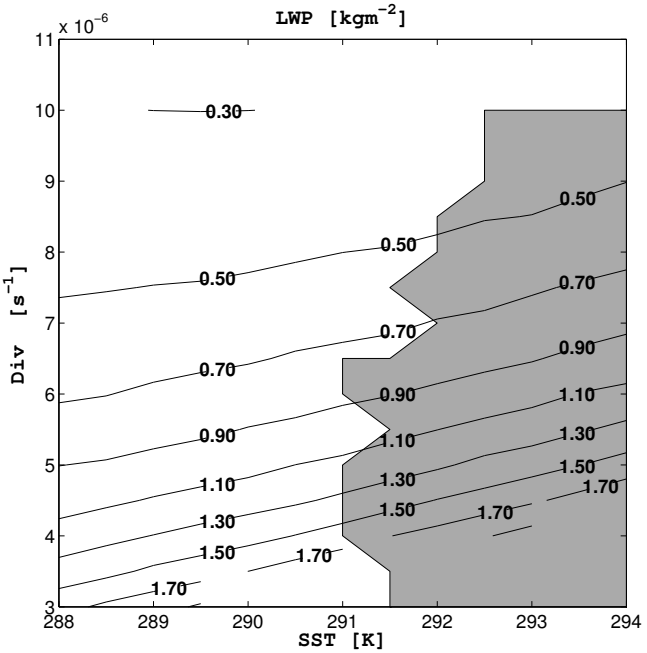

Figure 3.6. Contourplot of LWP in terms of divergence D and the sea surface temperature SST. The decoupled region is shaded gray. Boundary conditions used are depicted in Table 3.2.

3.3.2. Radiative cooling and SST

Increasing the (longwave) radiative cooling would result in more cloud top turbulence and would encourage an increasing inversion height. This is indeed what figure 3.7 shows. Changing the radiation from $20Wm^{-2}$ upwards results in an almost linearly increasing LWP. It shows that Sc formation is enhanced during the night, in which the nighttime averaged total radiation dF_{rad} is typically larger than during the day where shortwave radiation warms the top of the cloud layer. The effect of SST remains similar to what is seen in figure 3.6 and it mainly results in increasing LWP and eventually decoupling. Important to notice is that the gradient towards increasing SST is hardly altered by the increasing radiation, implying that the only consequence of increasing dF_L is cloud thickening by better mixing of the STBL.

3.3.3. Absolute velocity and SST

The influence of velocity $|\vec{U}|$ is significant. Noting that it has a strong effect on the surface fluxes $C_d|\vec{U}|\,(q_{t,0} - q_{t,ml})$ and $C_d|\vec{U}|\,(\theta_{l,0} - \theta_{l,ml})$. This will consecutively raise the mixed layer values towards their respective surface values as equations (2.37) and (2.38) have explained before. Figure 3.8 shows that the effect of $q_{t,ml}$ increasing is bigger than that of $\theta_{l,ml}$ as LWP typically increases for increasing $|\vec{U}|$. This effect is however only significant for higher SST. Nevertheless $\theta_{l,ml}$ to approach $\theta_{l,0}$ causes the BL to decouple and it is seen that this is the case for almost the entire plot.

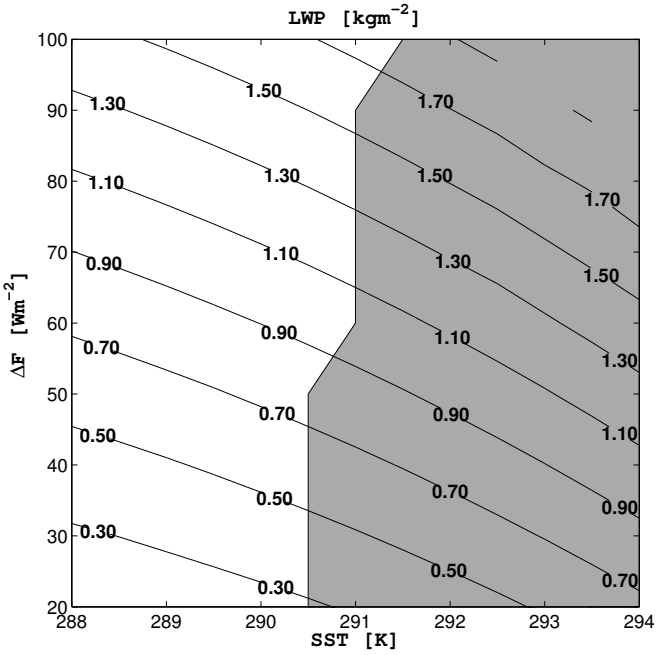

Figure 3.7. Contourplot of LWP in terms of radiative cooling dF_{rad} and the sea surface temperature SST. The decoupled region is shaded gray. Boundary conditions used are depicted in Table 3.2.

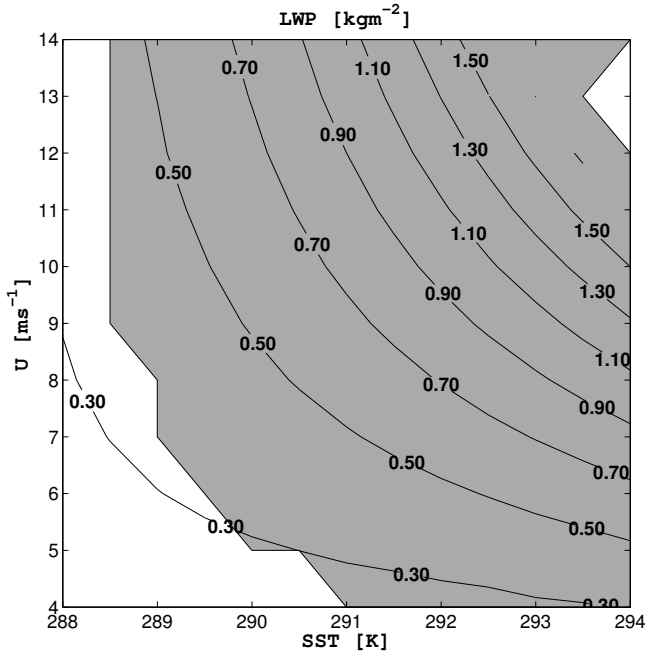

Figure 3.8. Contourplot of LWP in terms of velocity $|\vec{U}|$ and the sea surface temperature SST. The decoupled region is shaded gray. Boundary conditions used are depicted in Table 3.2.

3.3.4. Horizontal advection

Of interest in this research of the MLM and the steady-state solutions is to make the model as complete and realistic as possible. For this purpose the large-scale mean horizontal advection is introduced (see section 2.4.4) and it reads as follows:

$$\frac{d\theta_{l,ml}}{dt} = \frac{C_D|\vec{U}|(\theta_{l,0} - \theta_{l,ml}) + w_e\Delta\theta_l}{z_i} - \frac{\frac{1}{c_p\rho_0}dF_L}{z_i} - \vec{U}\frac{\partial\theta_l}{\partial x}$$

and

$$\frac{dq_{t,ml}}{dt} = \frac{C_D|\vec{U}|(q_{t,0} - q_{t,ml}) + w_e\Delta q_t}{z_i} - \vec{U}\frac{\partial q_t}{\partial x}.$$

These equations clearly show the horizontal advection serves as an extra source term. For the temperature tendency equation it results in extra cooling (or heating) and it will therefore have a clear influence on turbulence creation and decoupling. Now the humidity equation will also have a source term and its effect will be new and will mainly influence the cloud base height.

To find a magnitude for the advection a typical horizontal gradient for the SST is (section 2.4.4) $\frac{\partial SST}{\partial x} = 5.0 \times 10^{-6} Km^{-1}$. With an advective velocity $U = 7ms^{-1}$ this will lead to horizontal advection magnitudes of approximately $U\frac{\partial q_t}{\partial x} = 2.5 \times 10^{-7} gkgs^{-1}$ and $U\frac{\partial \theta_l}{\partial x} = 3.5 \times 10^{-6} Ks^{-1}$. If the MLM is now run till steady-state is reached profiles like in figure 2.3 are expected. To verify this behaviour a range of negative to positive SST-gradient is gone through and the effect is shown in figure 3.9 where the steady-state buoyancy flux for negative, positive and zero advection is plotted (-1 ,$+1$ and 0 times the above noted values). All other (fixed) variables are as in in Table 3.1. The buoyancy flux proves to be a way of immediately seeing inversion height, cloud base and subcloud and cloud fluxes and is therefore very illustrative.

It is seen that the positive advection has created a negative gradient in both subcloud and cloud fluxes; the negative advection a positive gradient. Most interesting is that the effect of the gradient of the subcloud flux to change the flux at cloud base is weaker than the effect of the advection itself on the surface flux. This has caused the positive advection to result in better mixing (less decoupling) as there is more turbulence and the negative advection to result in worse mixing (and eventually decoupling). In the remainder of this thesis the advection term, when used, will be considered positive as this is more realistic (especially in the Hadley circulation).

From the profiles is also seen that the the advection hardly changes the cloud base and inversion height. It only shows an effect on inversion and surface fluxes.

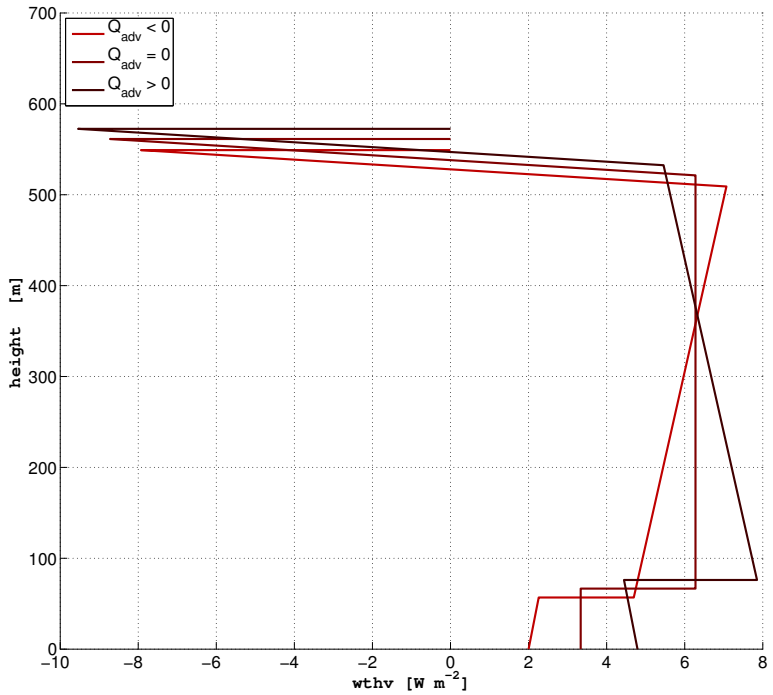

Figure 3.9. Steady-state buoyancy flux profiles for negative, zero and positive advection. Boundary conditions used are $\delta q_t = -8gkg^{-1}$ and $\delta\theta = 5K$ (these values are chosen to show a nice profile. Behaviour as observed for other free atmosphere conditions is roughly similar). Other boundary layer variables are depicted in Table 3.1.

Now that the horizontal advection can be used in the MLM the same analysis is done for increasing $|\vec{U}|$. If it is assumed that U increases as much as $|\vec{U}|$ an amplification of the advection term is expected. Figure 3.10 shows that there is no big effect on the behaviour of figure 3.8. The decoupled region has slightly decreased and LWP is just slightly lower. Overall it is concluded that the advection term results in a more realistic buoyancy flux profile but does not effect the STBL in any other significant way.

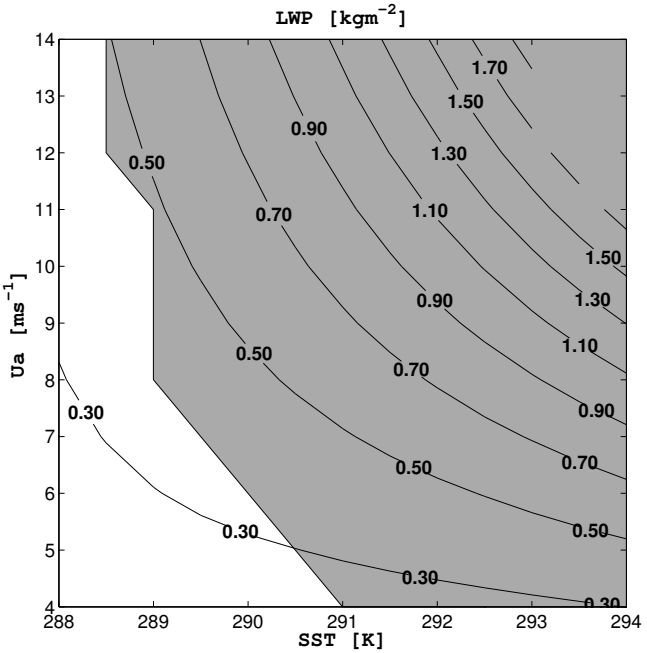

Figure 3.10. Contourplots of LWP in terms of absolute velocity $|\vec{U}|$ and the sea surface temperature SST. The decoupled region is shaded gray and the decoupling criterium is based on the temperature flux at cloud base. Boundary conditions used are depicted in Table 3.2.

Chapter 4

Climate change

The influence of Stratocumulus on the energy balance of the atmosphere is significant. It is therefore interesting to research the effect of a future climate on Sc. As it is expected that a future climate corresponds to a global positive temperature change the effect of this temperature change is investigated. It is related to a SST -increase of 2 degrees and, in particular, the change of cloud thickness is studied. Both the numerical and the analytical model will be used to analyse this behaviour. Within this investigation some key atmospheric boundary layer variables will be altered to see what effect they have on Sc evolution. Finally the MLM will be compared to steady-state solutions obtained with the Dutch Atmospheric Large Eddy Simulation (DALESv3.2) model [16]. These simulations, performed within the CGILS research [7], have perturbed the SST by 2 degrees.

In this chapter contourplots of the change in LWP due to the SST -increase of 2 degrees will be provided as a function of the different free atmosphere variables δq_t and $\delta\theta$. The SST-increase has as an effect that the equations for $q_{t,fa}$ and $\theta_{l,fa}$, (2.40) and (2.41), can be implemented in the MLM in two different ways: one in which $q_{ref} = 10.3gkg^{-1}$ and $\theta_{ref} = 286K$ are fixed and the other where the free atmosphere condition changes as much as the surface conditon, $q_{ref} = q_{t,0}$ and $\theta_{ref} = \theta_{l,0}$. With these implementations two situations are distinguished. The first resembles a situation where only $q_{t,0}$ and $\theta_{l,0}$ increase. An advantage of this is that it can, in some ways, be compared to the Hadley circulation where the STBL is advected towards warmer SST while the free atmosphere stays rougly constant. The other situation resembles a large scale situation where not only the ocean temperature has risen due to the climate change but the entire atmospheric condition.

Table 4.1. Reference values as used in this chapter. Results for this reference case are seen in figure 4.2.

variable	range / value	
SST	$[288, 290]$	K
$\delta\theta$	$[-2, 14]$	K
δq_t	$[-10, 0]$	gkg^{-1}
Γ_θ	6.0	Kkm^{-1}
Γ_q	0	$gkg^{-1}km^{-1}$
D	5.0	$\times 10^{-6}\ s^{-1}$
dF_{rad}	30	Wm^{-2}
$\lvert\vec{U}\rvert$	7.0	ms^{-1}
$\partial SST/\partial x$	0	Kkm^{-1}
p_0	1029	hPa

The following section will be devided into two parts: one for the now

so-called constant free atmosphere condition and one for the changing free atmosphere condition. In the first part results for a reference case will be provided in figure 4.2. This contourplot that shows the change $\Delta LWP/\Delta SST$ is created with a number of realistic reference values that are depicted in Table 4.1. To study how the different boundary layer variables influence the change $\Delta LWP/\Delta SST$ 6 perturbations are done to this reference case and are devided into 6 seperate experiments. These experiments are shown in Table 4.2.

In the second part the same reference case will be used to study the changing atmosphere condition; results are provided in figure 4.10. This part proves to be less sensitive to the different perturbations and will not be discussed in as much detail as the first part.

4.1. Numerical results

The numerical steady-state solutions are produced in the same manner as in chapter 3. For the analytical model the derivation as presented in Appendix A and section (3.2) is used. In this section first the numerical results are shown and are then explained by the aid of the analytical results.

4.1.1. Constant free atmosphere

Figure 4.2 shows $\Delta LWP/\Delta SST$ for the reference case (Table 4.1). In this plot and all further plots four regimes will be indicated: one for a decreasing LWP (unshaded), one for an increasing LWP (light gray), one for which the perturbed ($SST = 290K$) MLM is decoupled (dark gray) and one for which the unperturbed ($SST = 288K$) MLM is decoupled (darker gray). In all results the decoupled region is not valid in the MLM but can and will be loosely related to a region where there is Cu. Furthermore the decoupled region with the lighter dark shading represents a region that was not yet decoupled in the unperturbed MLM and has become decoupled in the perturbed MLM. This could therefore be related to a scenario where a transition from Sc to Cu has taken place. All these different regions would conclusively represent different changes of the cloud optical thickness and a different climate feedback.

Now looking at figure 4.2 it is noticed that there is a steep transition from a thinning cloud to a thickening cloud for decreasing atmospheric stability, as depicted by $\delta\theta$. But the dark shading in this region, where a thickening cloud is expected, actually denotes that the MLM is decoupled. Only for relatively moist free atmosphere conditions, low δq_t, there is thickening albeit very small. The decoupled region itself is as introduced divided into a part where there is a strong reduction in cloud optical thickness and where there is no change (or where the MLM is not valid at all). As expected from the results of section 3.3 it also shows that the increase in SST has resulted in a bigger region of decoupling..

To understand the behaviour of the LWP the competition between z_i and z_b, as introduced in section 1.3, is recalled. As expected from the behaviour in the Hadley circulation, where an increase in SST corresponds with an increase of the inversion base, were the cloud to thicken the increase of z_i has to be larger than that of z_b. Would z_b grow quicker than z_i the opposite would happen and the cloud thickness and thus LWP would decrease.

There are two effects that will determine what happens. The first effect is the influence on z_i. As z_i asymptotically increases for decreasing $\Delta\theta_l$ (see figure 3.1 and 3.3) a relatively high $\Delta\theta_l$ would dampen this increase. This is indeed seen clearly. The higher stability for high $\delta\theta$ resulting in a steadily increasing inversion corresponds with a negative $dLWP$. The influences on the cloud base are different. To understand this figure 4.1 is introduced.

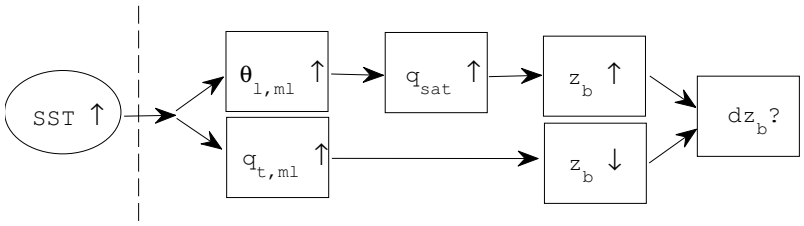

Figure 4.1. Block diagram that shows the respective terms that contribute in either a decrease or an increase of cloud base height z_b. The question asked is whether for an increasing SST the cloud base grows more than the inversion grows.

The figure tells that the change of z_b is determined by the competition of the humidity $q_{t,ml}$ and the temperature $\theta_{l,ml}$. An $SST-$increase respectively raises $\theta_{l,ml}$ and $q_{t,ml}$ in the boundary layer. As an increase of $\theta_{l,ml}$ increases the cloud base height and an increase of $q_{t,ml}$ actually lowers the cloud base height their combined effect determines what effectively happens. As z_i always increases for an SST-increase (for instance seen in the Hadley circulation) the cloud will only thin if the increase of z_b is bigger than that of z_i. For that to happen the growths of $\theta_{l,ml}$ and $q_{t,ml}$ should be such that the change of $\theta_{l,ml}$ results in a change of q_{sat} that is much bigger than the change of $q_{t,ml}$. It is therefore of importance to look at the respective factors that could further influence $\theta_{l,ml}$ and $q_{t,ml}$ and could finally result in a situation where z_b changes more than z_i. For that purpose all boundary layer variables will one by one be perturbed to see what effects they typically induce on the competition of z_i and z_b and on the competition of $q_{t,ml}$ and $\theta_{l,ml}$.

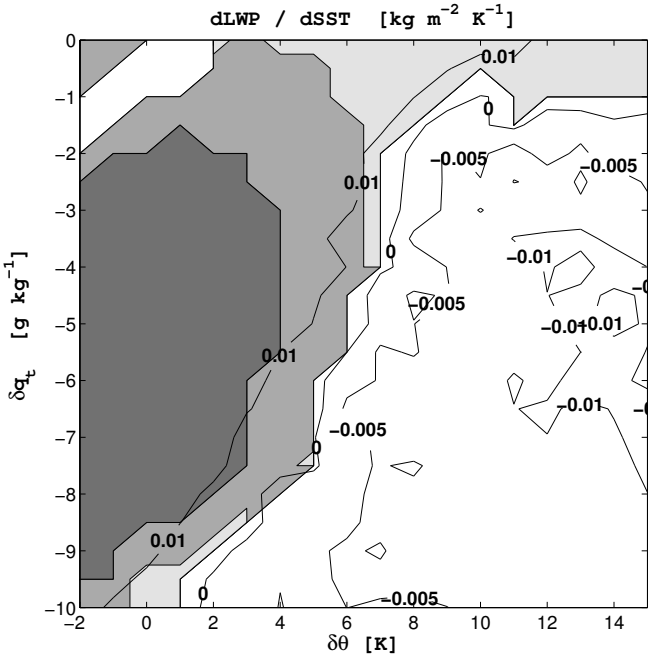

Figure 4.2. $\Delta LWP/\Delta SST$ for an increase of SST from $288K \rightarrow 290K$ with $dF_{rad} = 30Wm^{-2}$. Four regions are shaded: increasing LWP (light gray), decreasing LWP (unshaded), decoupled in the perturbed MLM (dark gray) and decoupled in both the unperturbed and perturbed MLM (darker gray).

4.1.1.1. Sensitivity analysis

By perturbing the reference case with conditions as in table 4.1 there are 6 variables of which their influence on z_i, $q_{t,ml}$ and $\theta_{l,ml}$ and thus on the change $\Delta LWP/\Delta SST$ can be studied: temperature lapse rate Γ_θ, humidity lapse rate Γ_q, divergence D, radiative cooling dF_{rad}, advective velocity $|\vec{U}|$ and horizontal advection $U\frac{\partial \psi}{\partial x}$. Their values will be perturbed as noted in table 4.2 and in the following figures their effect on the thickening and thinning regimes will be discussed by comparing the new contourplots with the reference plot in figure 4.2.

Table 4.2. Perturbed values of the boundary conditions for the 6 experiments. In each experiment one condition will be perturbed and the effect of perturbation will be studied by comparing it to Figure 4.2. All other (unperturbed) values are depicted in Table 4.1.

Exp.	Fig.	perturbed variable	value	
1	4.3a	Γ_θ	10	Kkm^{-1}
2	4.3b	Γ_q	-2.0	$gkg^{-1}km^{-1}$
3	4.4	D	10	$\times 10^{-6}\ s^{-1}$
4	4.5	dF_{rad}	70	Wm^{-2}
5	4.6	$\|\vec{U}\|$	12.0	ms^{-1}
6	4.7	$\partial SST/\partial x$	5.0	$\times 10^{-6}\ Kkm^{-1}$

Free atmosphere lapse rates Γ_θ and Γ_q
The influence of Γ_θ is apparent from the much bigger region of cloud thinning and the complete absense of a thickening region (this region is completely decoupled). Furthermore the region of decoupling itself has decreased in size due to the higher stability of the atmosphere $\Delta\theta_l$ (due to the increased lapse rate). Γ_θ limits the growth of z_i for an increase in SST resulting in a bigger region where z_b increases faster than z_i and the cloud thins.

Now it is surprising to note the effect of Γ_q in the right plot. It seems to almost have the same effect as Γ_θ but obviously there must be a different cause. Now the inclusion of Γ_q has resulted in a much stronger dependency of the humidity on the inversion height z_i, as was concluded for case 2 of section 3.1. Now, as z_i has increased due to the SST-increase, the free atmosphere humidity $q_{t,fa}$ just above the inversion has become drier. As this has a direct drying effect on $q_{t,ml}$ because drier air is now entrained into the boundary layer, referring figure 4.1, z_b has now risen more than before. As a result z_b has now more often won the competition with z_i.

It can be concluded that the lapse rates both have a strong effect on the cloud evolution but by very different causes.

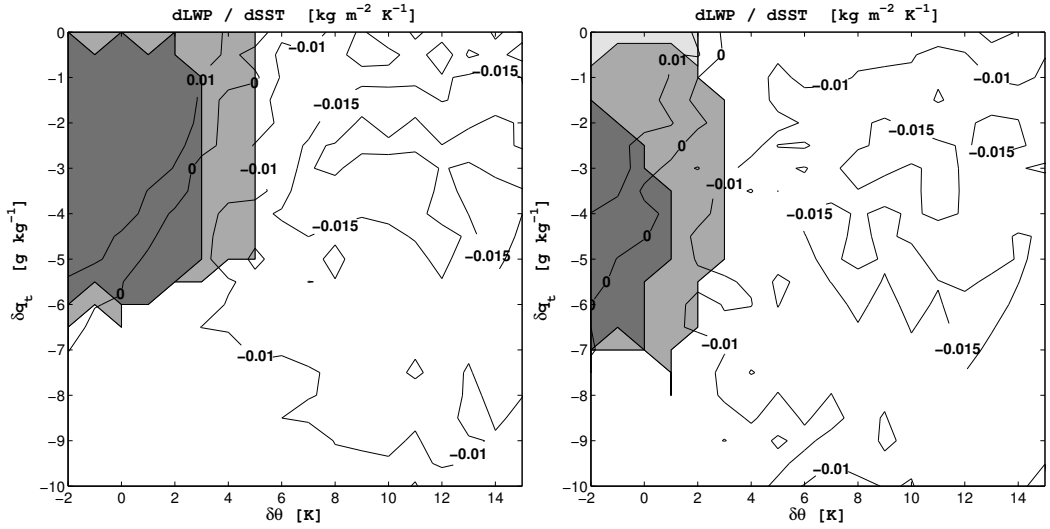

Figure 4.3. $\Delta LWP/\Delta SST$ plots for (on the left) $\Gamma_\theta = 10Kkm^{-1}$ and (on the right) $\Gamma_q = -2gkg^{-1}km^{-1}$. Other variables are denoted in Table 4.1.

Divergence D

Figure 4.4 shows the effect of a higher divergence. The same behaviour as before is observed: the plot shows a steep transition between thinning and decoupling and again there is a very small region where the STBL is not decoupled but the cloud does thicken. Most importantly the region of thinning is a lot bigger. This is obviously caused by the larger divergence pressing down on the boundary layer, thus serving the same purpose as a larger $\Delta\theta_l$: damping the growth of z_i.

Furthermore the decoupled region has been supressed a lot. Surely the parameter D stabilizes the $STBL$ by resulting in an overall lower z_i.

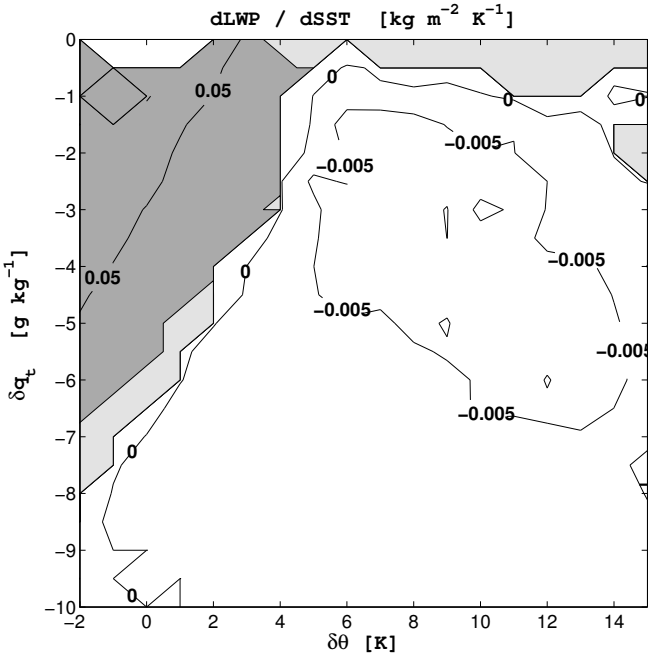

Figure 4.4. Contourplots of $\Delta LWP/\Delta SST$ for $D = 10 \times 10^{-6}s^{-1}$. Other variables are denoted in Table 4.1.

Radiative cooling dF_{rad}

Now the effect of a higher radiative cooling is addressed. Where the value $dF_{rad} = 30Wm^{-2}$ was chosen as to represent a net daily radiative cooling, taking into account shortwave radiation during the day, now the new value would (as in section 3.1) again represent a nocturnal Sc. The plot in figure 4.5 shows that the higher cooling does not change the transition line much, but it does effect the magnitude of cloud thinning. The higher radiative cooling resulting in a higher inversion ($z_i \propto dF_L$) and a lower cloud base ($z_b \propto \theta_{l,ml}$ for constant $q_{t,ml}$) increases magnitudes of change but apparently it hardy effects the transition line.

Furthermore, as obviously the larger radiative cooling creates more turbulence, the decoupled region has decreased. This results in a bigger region in which the cloud actually becomes thicker instead of the boundary layer becoming decoupled; an effect that tells that indeed Sc formation is enhanced during the night.

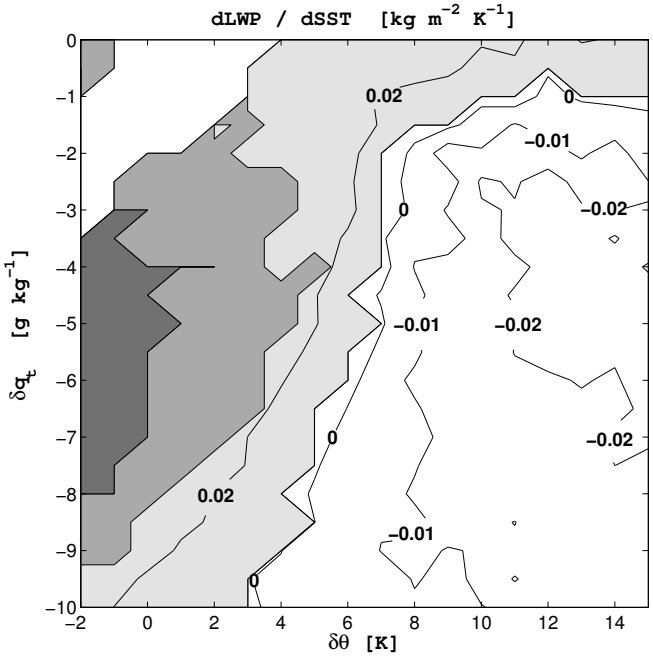

Figure 4.5. Contourplots of $\Delta LWP/\Delta SST$ for for $dF_L = 70Wm^{-2}$. Other variables are denoted in Table 4.1.

Absolute velocity $|\vec{U}|$

The effect of increasing $|\vec{U}|$ is that it will force both $q_{t,ml}$ to $q_{t,0}$ and $\theta_{l,ml}$ to $\theta_{l,0}$. This significantly influences the steady-state solutions as no transition line is found and the entire regime is shifted to where the cloud thickens and the boundary layer is eventually fully decoupled.

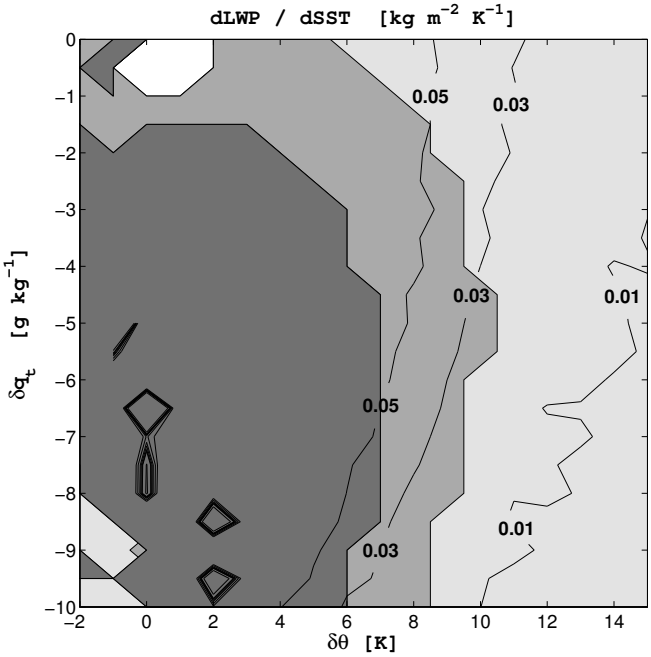

Figure 4.6. Contourplot of $\Delta LWP/\Delta SST$ for $|\vec{U}| = 12ms^{-1}$. Other variables are denoted in Table 4.1.

Horizontal advection

Figure 4.7 shows the effect of horizontal advection invoked by a SST-gradient of $\frac{\partial SST}{\partial x} = 5 \times 10^{-6} Km^{-1}$. It effects the STBL in the same way as the longwave radiative cooling does (there is extra cooling), except that now there is an extra source term for the humidity. Apparently this counters the the effect of the cooling as figure 4.7 shows that the region of decoupling is basically the same as in the reference figure 4.2. As was shown in section 3.3 the effect of the horizontal advection is not significant.

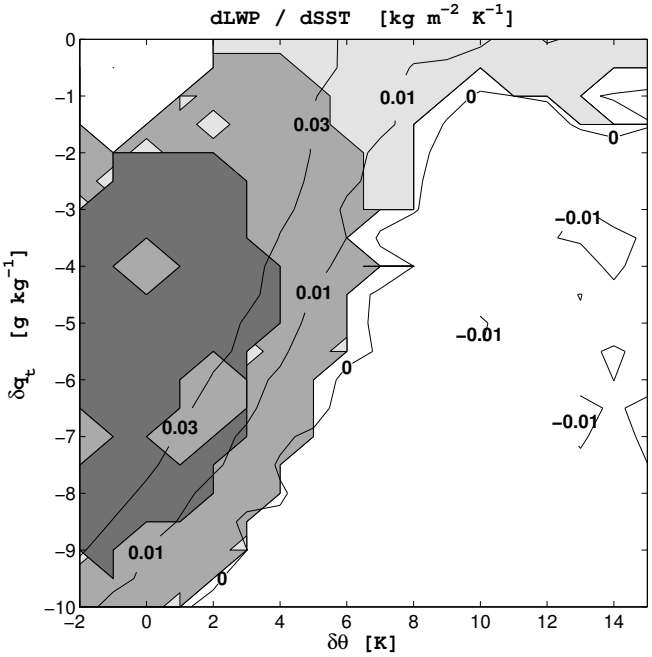

Figure 4.7. Contourplots of $\Delta LWP/\Delta SST$ with horizontal advection due to a $\frac{\partial SST}{\partial x} = 5{\times}10^{-3}Kkm^{-1}$. The decoupling criterium is now based on the temperature flux at cloud base: $\overline{w'\theta'_v}|_{z_b} < 0$. Other variables are denoted in Table 4.1.

With horizontal advection now also a new plot for the influence of $|\vec{U}| = 12ms^{-1}$ is presented in figure 4.8. Here too no strong effect is noticed due to the extra advection on the change in LWP due to the stronger velocity.

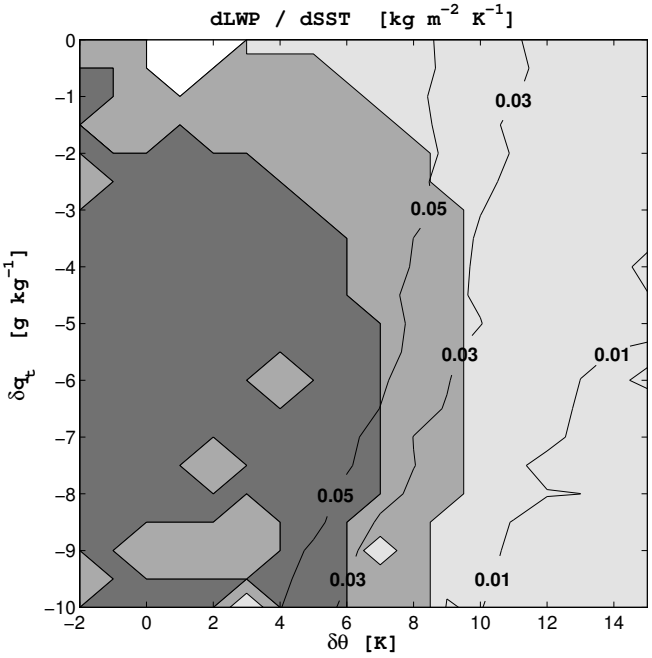

Figure 4.8. Contourplots of $\Delta LWP/\Delta SST$ horizontal advection due to a $\frac{\partial SST}{\partial x} = 5 \times 10^{-3}Kkm^{-1}$ for $|\vec{U}| = \vec{U} = 12ms^{-1}$. The decoupling criterium is now based on the temperature flux at cloud base: $\overline{w'\theta'_v}|_{z_b} < 0$. Other variables are denoted in Table 4.1.

4.1.1.2. Behaviour of inversion and cloud base

To explain the behaviour that effectively results in either a thickening or a thinning cloud the evolution for increasing SST of the parameters z_i, z_b, $q_{t,ml}$, $\theta_{l,ml}$ and q_{sat} is shown in figure 4.9. To arrive at this plot two points, one where the cloud thickens and one where the cloud thins, were picked in figure 4.5 (as this figure most clearly showed both scenarios). The following coordinates $\{\delta\theta; \delta q_t\}$ are used: $\{2K; -9gkg^{-1}\}$ where the cloud thickens and $\{12K; -5gkg^{-1}\}$ for where the cloud thins.

The figure first shows that the boundary layer becomes warmer as $\theta_{l,ml}$ linearly increases with increasing SST, for both cases. This subsequently causes q_{sat} to grow increasingly stronger as the boundary layer becomes warmer as q_{sat} possesses an exponential behaviour for higher temperatures (figure 2.4). This, as $q_{t,ml}$ only increases linearly, will raise z_b in all cases. The thickening of the cloud nevertheless is mostly caused by the ever increasing inversion and this increase is stronger for the case with the lower atmospheric stability $\delta\theta$. Ultimately these combined effects result in a thickening and a thinning scenario, as seen in the rightmost graph. There it is observed that the decrease in LWP is actually very minor, as the ΔLWP plots have showed before, and that eventually even a slight increase is noticed. In any case the difference in behaviour of the cloud is very significant.

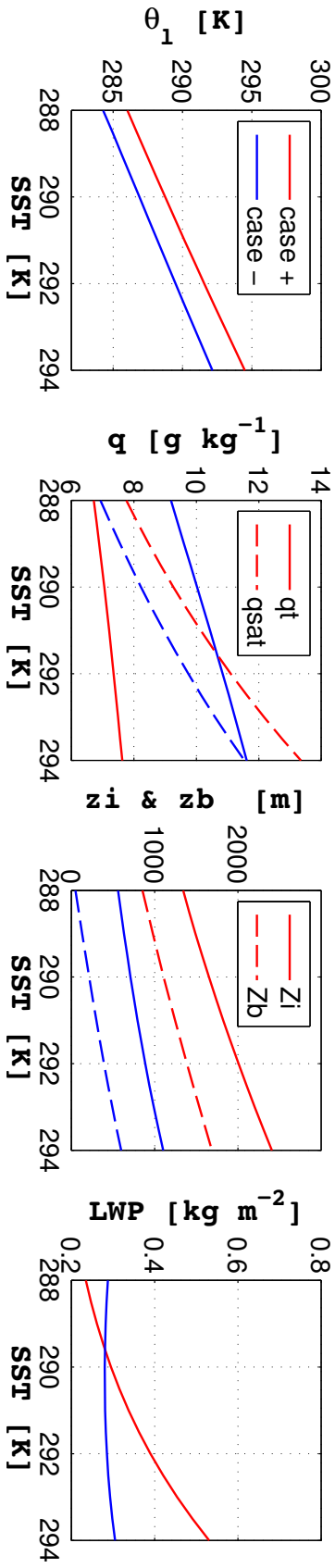

Figure 4.9. Figure of the evolution of boundary layer variables that determine whether the cloud thickens or thins. The red line denotes the thickening scenario with conditions $\{\delta\theta = 2K; \delta q_t = -9gkg^{-1}\}$ and the blue line the thinning scenario with conditions $\{\delta\theta = 12K; \delta q_t = -5gkg^{-1}\}$. The conditions used are as in table 4.2 with $dF_L = 70Wm^{-2}$ (the latter is used to have a clearer thickening region).

4.1.2. Changing atmosphere

Now the other case will be looked at. The main difference with the previous case is that the free atmosphere now also changes due to the increasing SST: $\theta_{ref} = \theta_{l,0}$. This causes the free atmosphere condition to change just as much in magnitude as the surface value. Effectively this will cause $\theta_{l,ml}$ to change as much as the surface value as equation (2.38) predicts (this will be explained in section 4.2).

Due to this behaviour $\Delta\theta_l$ will remain approximately constant and therefore the inversion height will too. As most variables strongly depend on z_i this implication has a large consequence: $q_{t,ml}$ and $\theta_{l,ml}$ will mostly depend on the surface values $q_{t,0}$ and $\theta_{l,0}$. A change of cloud thickness is therefore only caused by the respective changes of $q_{t,0}$ and $\theta_{l,0}$ due to the SST-increase.

Figure 4.10 shows the huge effect of this implication. Either the cloud thickens or the boundary layer is decoupled. Apparently the fact that z_i hardly changes also strongly effects z_b. This is directly caused by the fact that both $q_{t,ml}$ and $\theta_{l,ml}$ change as much as their surface values. To explain this it is again related to the change of q_{sat} at cloud base and the change of $q_{t,ml}$. The change in $q_{t,ml}$ is directly related to the change in $q_{t,0}$ and this is evaluated from the SST-increase, while the change of q_{sat} at cloud base is determined by the change of $\theta_{l,ml}$. While both changes in temperature are equal the fact that q_{sat} is evaluated at a higher altitude (lower temperature) results in this change to be slightly smaller than the change of $q_{t,ml}$ due to the exponential behaviour of q_{sat} towards higher temperature (figure 2.4).

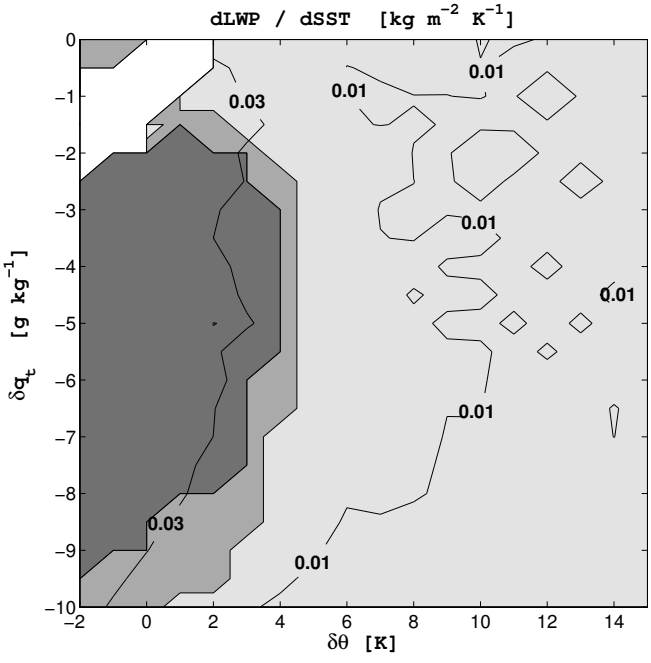

Figure 4.10. Contourplot of $\Delta LWP/\Delta SST$ for the changing atmosphere condition. Conditions as in case 1 with $dF_L = 30 Wm^{-2}$.

4.2. Analytical results

To understand the results of section 4.1 it is important to analytically study the changes of z_i and z_b due to an increase in SST: $\frac{\partial z_i}{\partial SST}$ and $\frac{\partial z_b}{\partial SST}$. Knowing the changes in both z_i and z_b due to the SST-increase the evolution of the cloud thickness $z_i - z_b \propto LWP$ is found. This section will therefore be used to gain further understanding of the behaviour as presented in section 4.1 by calculating the combined derivative

$$\frac{\partial z_{cld}}{\partial \theta_{l,0}} = \frac{\partial z_i}{\partial \theta_{l,0}} - \frac{\partial z_b}{\partial \theta_{l,0}}. \tag{4.1}$$

for the familiar set of boundary conditions (table 4.1). The derivative with respect to $\theta_{l,0}$ will be taken instead of the SST. This causes just a difference of a factor equal to the Exner function $\Pi \approx 1$, but makes the calculations slightly easier. This will be done for both the constant and the changing atmosphere and it will be checked if the sign of $\partial z_{cld}/\partial \theta_{l,0}$ verifies the tendency as found in the solutions of the numerical model.

4.2.1. Constant free atmosphere

Differentiating the known equation for z_i , eq. (A.11), with respect to $\theta_{l,0}$ gives equation (A.14):

$$\frac{\partial z_i}{\partial \theta_{l,0}} = \frac{1}{2\Gamma_\theta}\left(\frac{\theta_{l,0}-\theta_{ref}-\delta\theta+\frac{(A-1)dF_L}{C_d|\vec{U}|}}{\sqrt{(\theta_{l,0}-\theta_{ref}-\delta\theta+\frac{(A-1)dF_L}{C_d|\vec{U}|})^2+\frac{4AdF_L\Gamma_\theta}{D}}}+1\right).$$

This differential equation already provides useful information about the behaviour of z_i for increasing temperature. As explained in equation A.11 z_i is proportional to $\theta_{l,0}$. The differential equation furthermore says that as z_i becomes higher the magnitude of change becomes higher which verifies that z_i grows stronger the higher it becomes. By combining this derivative with that of z_b the tendency for the Sc can be predicted given the set of boundary conditions. To see if the analytical model can also predict some of the behaviour as found in section 4.1 therefore another contourplot is provided in figure 4.11 below. All values used are as for Exp. 2, denoted in Table 4.2. This particular experiment, with $\Gamma_q = -2gkg^{-1}km^{-1}$, is chosen as it includes all parameters of the STBL and because it results in the most clear regimes of thickening and thinning.

A transition line with similar behaviour as before is noticed, only located further to the right for higher $\delta\theta$. It is actually the case that were the cloud to thin this magnitude is very small. Most of the thinning regime can therefore be interpreted as where the cloud stays nearly equal in thickness. The fact that z_b can never change that much that it totally overcomes the growth of z_i is most probably caused by the entrainment parameterization that does not take the humidity jump into account, and therefore is not influenced extra by a drier free atmosphere.

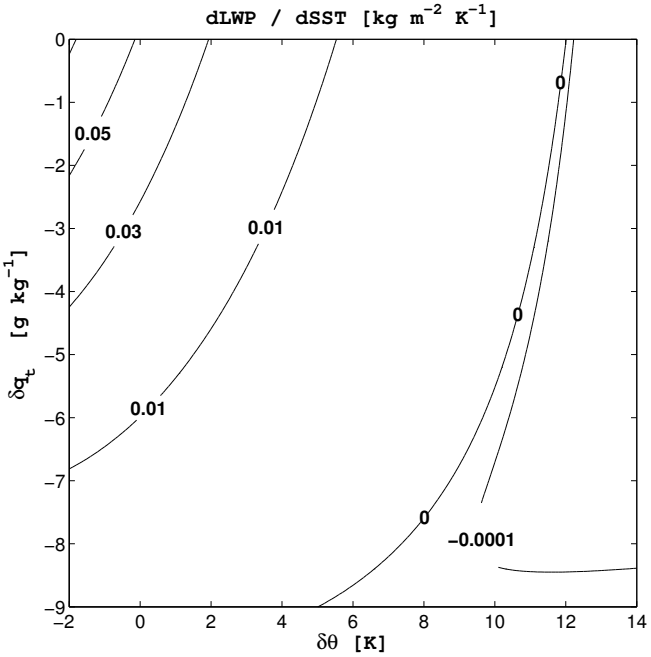

Figure 4.11. Contourplot of $\Delta LWP/\Delta SST$ for the analytical MLM. Conditions are those of Exp. 2, Table 4.2.

4.2.2. Changing free atmosphere

Substituting the equality $\theta_{ref} = \theta_{l,0}$ for the changing free atmosphere condition in the equation for z_i (Eq. A.11) gives an expression for z_i that is independent of $\theta_{l,0}$:

$$z_i = \frac{1}{2\Gamma_\theta}\left[\frac{(A-1)F'}{C_d|\vec{U}|} - \delta\theta\right] + \frac{1}{2\Gamma_\theta}\sqrt{\left(\frac{(A-1)F'}{C_d|\vec{U}|}\delta\theta\right)^2 + \frac{4AF'\Gamma_\theta}{D}}. \quad (4.2)$$

This independency directly verifies the behaviour found in section 4.1.2 that the inversion stays constant if the free atmosphere temperature changes as much as $\theta_{l,0}$. The implication of this independency on $\theta_{l,0}$, as expected, influences the steady-state solutions for $q_{t,ml}$ and $\theta_{l,ml}$ very much. By substituting $\psi_{fa}$the equalities $w_e = Dz_i$ and $q_{t,ref} = q_{t,0}$ into equations (2.37) and (2.38) the following equations result:

$$\theta_{l,ml} = \theta_{l,0} + \frac{Dz_i(\delta\theta + \Gamma_\theta z_i) - F'}{C_d|\vec{U}| + Dz_i} \quad (4.3)$$

and

$$q_{t,ml} = q_{t,0} + \frac{Dz_i(\delta q_t + \Gamma_q z_i)}{C_d|\vec{U}| + Dz_i}. \quad (4.4)$$

It is immediately observed that both mixed values are directly determined by the surface value. Calculating the derivatives furthermore shows that the changes in $\theta_{l,ml}$ and $q_{t,ml}$ are equal in magnitude to the changes in the surface values $\partial\theta_{l,0}$ and $\partial q_{t,0}$. This implies that calculating the derivative for z_b (Eq. (2.66)) $\partial z_b/\partial SST$ has become quite simple and results in:

$$\frac{\partial z_b}{\partial SST} = -2\frac{L_v}{R_v}\frac{SST}{g/c_p} ln\left(1 + \frac{Dzi(\delta q_t + \Gamma_q z_i)}{Dz_i + C_D|\vec{U}|}\right). \tag{4.5}$$

As the term within the logarithm $1 + \frac{Dzi(\delta q_t + \Gamma_q z_i)}{Dz_i + C_D|\vec{U}|} > 1$, except for high negative Γ_q which results in an unrealistic negative $q_{t,fa}$, the tendency for z_b will always be decreasing, hence the thickening of the cloud for all boundary conditions. This compares very well with the results obtained with the numerical model which also predicts a thickening cloud for all conditions. It seems the implementation of a constant z_i has some very significant effects.

4.3. CGILS - MLM comparison

The analysis as done in the previous section is inspired by CGILS [7]. To validate the results of the MLM and to compare the CGILS LES results (as simulated by DALESv3.2 [**?**]) with those of the MLM the initial surface and free atmosphere conditions of two cases, S11 (Stratocumulus) and S12 (Stratus), will be used as input for the MLM. As both cases possess horizontal advection this term is added to the MLM as explained in section 2.4.4.

Two simulations will be compared: One at a control climate with respectively (for S11 and S12) $SST = 292.5K$ and $SST = 291K$ and one at the so-called perturbed climate where the SST is increased by two degrees.

S11 (Stratocumulus)

Figure 4.12 shows the respective profiles of q_t, θ_l and $\overline{w'\theta_v'}$ for the MLM and LES simulations. First thing that is noticed when looking at the mixed layer profiles is the discrepancy between the profiles of q_t. For the LES the boundary layer seems not well mixed and the profiles therefore differ by quite a margin. For θ_l this is not the case. The mixed layer value is represented very well. Another difference is the underpredicted inversion height for the MLM, probably caused by the main difference in how the models are setup: the MLM uses a parameterization while the LES does not. In any case for all variables their increase in the perturbed simulation is similar. This is encouraging as it shows that overall the change and thus the actual effect of the SST is caught quite well.

The buoyancy-flux profiles are very different but the subcloud layer shows reasonable similarity. In particular they both show a decoupled boundary layer as seen in the negative buoyancy flux at cloud base. This means that the MLM , as seen in the ΔLWP plots of section 4.1, would predict quickly increasing LWP. This is indeed what is seen in Table 4.3 where the values of LWP, $\Delta\theta_l$, Δq_t, z_i and z_b for the four simulations, and their respective changes, are shown. It however does not agree with the negative change in LWP of the LES. Noted can be though that the LWP of both models itself does not agree at all: they differ by a factor of 10. However, the change in actual cloud thickness $z_i - z_b$ is similar. This big difference in behaviour for LWP and cloud thickness is caused by the already unrealistic decoupled STBLs for both models, that predict a much different z_b. Referencing the results of section 4.1 it can be said though that, while the LES is still valid, the MLM is not valid (see [11]), as it is decoupled, but can meanwhile be interpreted as in a transition to Cu. This does correspond with a decrease in cloud cover and thus with a negative feedback, like the LES predicts.

Nevertheless it is more useful to move on to the Stratus simulations at S12 in the next subsection where, as will be shown, all simulations result in a coupled BL and it will be much more interesting to do the comparison.

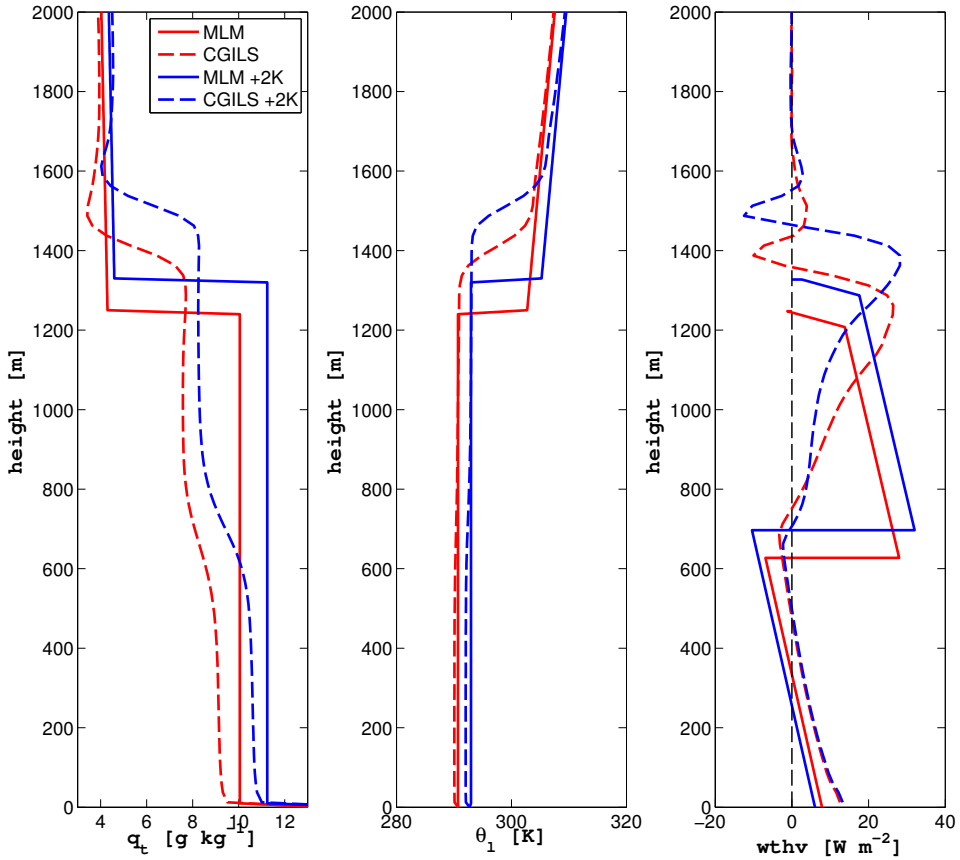

Figure 4.12. Profiles of q_t, θ_l and $\overline{w'\theta'_v}$ for the MLM (solid line) and DALES (dashed line) for the control and perturbed climate.

Table 4.3. Predictions of boundary layer variables for S11. Given are the values for the control (CTL) and perturbed (P2K) climate as well as the difference Δ as predicted by the Mixed Layer Model and DALES 3.2.

Model	LWP $[kgm^{-2}]$	$\Delta\theta_l$ $[K]$	Δq_t $[gkg^{-1}]$	z_i $[m]$	z_b $[m]$	$z_i - z_b$ $[m]$
MLM CTL	0.435	12.01	-5.85	1250	627	623
DALES CTL	0.041	12.50	-3.81	1386	1137	249
MLM P2K	0.466	12.25	-6.65	1328	697	631
DALES P2K	0.031	12.90	-3.71	1509	1256	253
Δ MLM	$+0.031$	$+0.24$	$+0.80$	$+78$	$+70$	$+8$
Δ DALES	-0.001	$+0.40$	-0.10	$+123$	$+119$	$+4$

S12 (Stratus)

S12 relates to Stratus clouds. These clouds are roughly identical to Sc but are lower lying and therefore much more stable and most of all coupled. This is seen in figure 4.13 which again shows the three profiles.

Here q_t is again overpredicted quite severely, eventhough this time the LES is very well mixed. θ_l is predicted as well as before as is the difference in inversion height z_i. As the latter difference is similar it can indeed be blamed on the entrainment parameterization.

The buoyancy flux is what is most interesting to notice for S12. The subcloud flux is almost exactly the same: it has the same gradient and magnitude up to the MLM cloud base. Furthermore the cloud layer is also represented much better which results in the much better predicted LWP as seen in Table 4.4, as is z_b.

The change in LWP nonetheless does not share the same sign. The LES predicts a thinning cloud, while the MLM predicts a slightly thickening cloud. Still it is encouraging. First of all the positive change in LWP is much smaller than before. Secondly the more positive change of z_b for the LES is probably just caused by the fact the MLM overpredicts $q_{t,ml}$ and also its change $dq_{t,ml}$. Therefore, while for the LES z_b wins the battle with z_i as in figure 4.1, in the MLM z_b changes less and the changes of z_b and z_i are equal, resulting in an almost constant thickness.

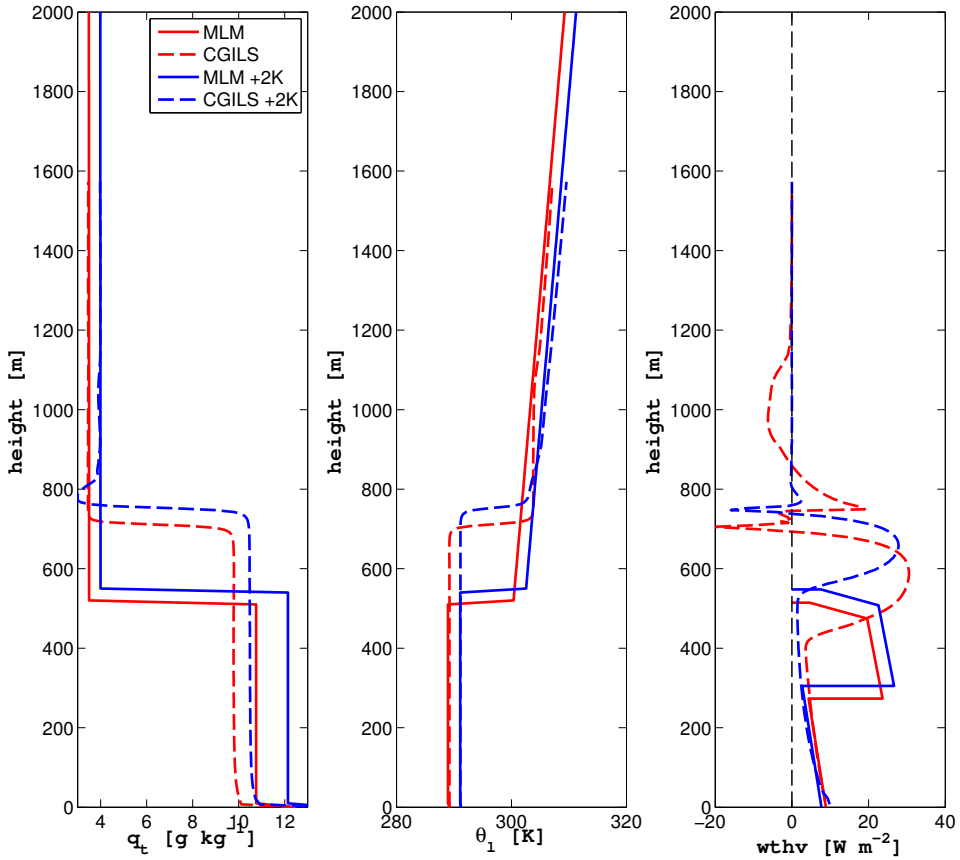

Figure 4.13. Profiles of q_t, θ_l and $\overline{w'\theta'_v}$ for the MLM (solid line) and DALES (dashed line) for the control and perturbed climate.

Table 4.4. Predictions of boundary layer variables for S12. Given are the values for the control (CTL) and perturbed (P2K) climate as well as the difference Δ as predicted by the Mixed Layer Model and DALESv3.2.

Model	LWP $[kgm^{-2}]$	$\Delta\theta_l$ $[K]$	Δq_t $[gkg^{-1}]$	z_i $[m]$	z_b $[m]$	$z_i - z_b$ $[m]$
MLM CTL	0.069	11.4	−7.30	515	273	242
DALES CTL	0.064	14.6	−6.33	710	465	255
MLM P2K	0.073	11.4	−8.11	548	306	242
DALES P2K	0.031	13.2	−6.42	751	578	173
Δ MLM	+0.004	0	+0.81	+33	+33	0
Δ DALES	−0.033	−1.4	+0.09	+41	+113	−72

Chapter 5

Conclusions and recommendations

This master's thesis has provided results obtained with a numerical and analytical mixed layer model for the Stratocumulus-topped boundary layer. The influences of free atmosphere conditions and of an increasing SST on steady-state solutions of the turbulent boundary layer have been thoroughly studied. This final chapter will therefore treat the conclusions that can be drawn from the results and will present some recommendations for future research.

5.1. Conclusions

5.1.1. Numerical and analytical Mixed-Layer Model

The mixed layer model as presented in this thesis was used to study the steady-state behaviour of the STBL. Using a proper entrainment parameterization that closes the three mixed layer equations for z_i, $q_{t,ml}$ and $\theta_{l,ml}$ steady-state solutions were found. First of all, by using the Nicholls Turton parameterization, numerical convergence of these equations resulted in these solutions. It showed that realistic boundary layer conditions can be properly predicted. Secondly, by using a simple entrainment parameterization that has been deduced from the parameterization of Moeng an analytical model was created. This model was used to quantitatively explain results of the numerical model and to provide a simple way of quantitatively studying steady-state solutions. The model nevertheless lacked in its performance by neither being able to predict decoupling nor not being able to adequately account for the inversion jump of humidity.

5.1.2. Free atmosphere conditions

A complete description of the free atmosphere conditions based on the parameters $\delta\theta$, δq_t, Γ_θ and Γ_q was setup. They were used to show that the influence of free atmosphere conditions on the amount of clouds in the boundary layer is significant. While the stabilizing influence of the free atmosphere potential temperature was known before it was now shown that changing the free atmosphere humidity too directly effects the thickness of Sc clouds. It was also demonstrated that the free atmosphere lapse rates of humidity and temperature give the boundary layer a strong dependency on the inversion height. Here a large temperature lapse rate dampens the growth of the mixed layer and the humidity lapse rate makes the free atmosphere increasingly drier for increasing inversion height.

5.1.3. Sensitivity analysis

Besides the free atmosphere conditions the parameters $|\vec{U}|$, D and dF_{rad} have important effects on the STBL. $|\vec{U}|$ significantly raises cloud thickness and eventually decouples the boundary layer as the mixed layer values of q_t and θ_l converge to their surface conditions. D stabilizes the STBL in the same way as the inversion jump $\Delta\theta_l$ and is an important measure for the entrainment in steady-state where subsidence exactly balances the entrainment. dF_{rad} determines a strong criterium for when decoupling occurs. Furthermore the large scale mean horizontal advection, $U\frac{\partial q_t}{\partial x}$ and $U\frac{\partial \theta_l}{\partial x}$, has been included in the numerical model. It has made the model more realistic as the vertical flux profiles of q_t and θ_l now obtained a gradient equal to the magnitude of advection.

Most important was the influence of the sea surface temperature SST. It was shown that it effects the thickness of the Sc and that the evolution of the cloud was controlled by the respective growths of the inversion z_i and cloud base z_b. The growth of the cloud base itself was furthermore controlled the competition of an increasing humidity that enhances cloud formation and an increasing temperature that diminishes cloud formation.

5.1.4. The influence of a future climate

The main focus of this thesis was on how different parameters influence the evolution of the STBL towards a future climate. By increasing the SST a future climate was simulated and by plotting the change in the Sc thickness it was shown that, strongly dependent on all the different parameters, there are four scenarios possible that can be related to either a positive or a negative feedback on the radiative balance of the atmosphere. A first case in which only the SST changes and the free atmosphere condition remains equal to the condition before the change of the SST has resulted in the scenarios shown in Figure 5.1 and summarized below:

1. The stratocumulus grows thicker: negative feedback
2. The stratocumulus grows thinner: positive feedback
3. The boundary layer becomes decoupled and the stratocumulus transitions into cumulus: very strong positive feedback
4. The boundary layer is already decoupled and remains decoupled

Of these scenarios in particular those where the stratocumulus grows thinner or where it is decoupled represent the dominant behaviour. The thickening region is hardly observed and only occurs in the nighttime when there is larger radiative cooling.

A second case in which the surface as well as the free atmosphere condition changes proved to be much less sensitive to the different boundary layer variables and only a decoupled or a thickening boundary layer was found.

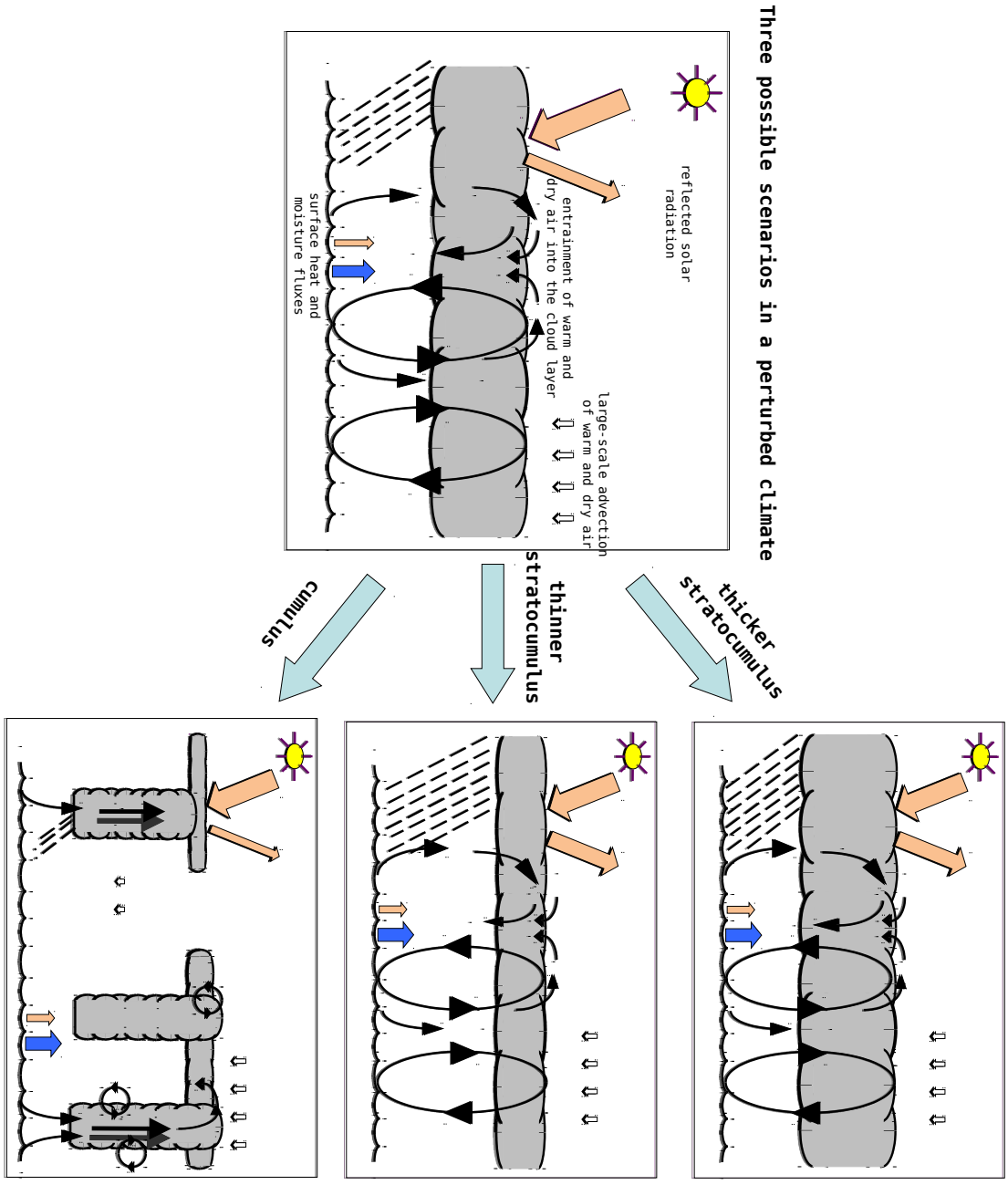

Figure 5.1. Schematic view of the three possible scenarios for stratocumulus in a perturbed climate. The stratocumulus as shown in the left figure either evolves into a thicker stratocumulus, a thinner stratocumulus or into cumulus. The first corresponds with a negative feedback, the latter two with a positive feedback.

5.2. Outlook and recommendations

5.2.1. CGILS

First of all it would be interesting to also perform the analyses as done with the MLM with the different single column models as used in the CGILS project. These extra results would, together with the framework that this research has provided, provide extra insight in why the cloud radiative feedback in the results of climate models differ by so much [1]. It will be interesting to relate these differences to the parameters that have shown to be of so much importance for the evolution of the cloud.

Furthermore this thesis has shown that the difference in how the free atmosphere condition changes and how the surface condition changes due to an SST-increase is of big importance. The CGILS research as currently being performed uses a free atmosphere condition in which the free atmosphere humidity changes less than the surface humidity while the free atmosphere temperature changes as much as the surface temperature. It could however be hypothesized that there are different relative changes possible of both values which then would result in much different results, as chapter 4 has shown. More knowledge about what happens to the entire atmospheric condition in a future climate should be obtained to more realistically predict the exact effect of an increasing SST. Performing more simulations with the different single column models for different free atmosphere conditions (and especially that of humidity) would be a means of obtaining this extra knowledge.

5.2.2. Analytical research

The analytical model as developed in this research has shown to be very useful in interpreting some of the more detailed numerical results. Still much more could be done with it. For instance it could efficiently be used to create some very interesting criteria related to the many competing processes that take place in the STBL. For one it would be interesting to find a transition point for which the respective changes of the cloud base and the inversion are equal: $\frac{\partial z_b}{\partial SST} = \frac{\partial z_i}{\partial SST}$. Finding this point would set a criterium for when the cloud would grow thicker or thinner. Another transition point would be where $z_b = z_i$ beyond which there would be no Sc possible. The same can be said for a point beyond which there would always be decoupling. This could be done, not only for an increase of the SST but also for other relevant parameters

5.2.3. Extension of the MLM

The MLM as used in this research is almost as complete as it could possibly be but there are still some features that have not been researched yet. For instance there is the influence of a diurnal cycle on the steady-state solutions. While the MLM would become decoupled at daytime for most simulations there could possibly be a regime in which the magnitude is sufficiently small that the MLM would be valid during the entire day. By researching daily averaged equilibrium states more realistic behaviour can be analysed.

Another feature that has not been used is precipitation. It would be of interest to see whether it would influence the steady-state solutions as the

other parameters do. It might possibly stimulate the clouds towards one of the possible scenarios depicted in section 5.1.

Finally the implementation of horizontal advection in the MLM of this research could be extended. Now it is assumed that both the horizontal gradients of humidity and temperature are caused by the same SST-gradient. It could however be that both gradients have different sources or that one of them is sufficiently stronger than the other. In order to catch the exact effect of horizontal advection some more thorough research should be done than is done in this thesis.

Appendix A

Derivation analytical solution

Below the derivation of the analytical solutions of the MLM as used in sections 3.2 and 4.2, found by using the assumption that the entrainment can be represented such:

$$w_e = \frac{AF'}{\Delta\theta_l}, \tag{A.1}$$

where $F' = dF_L/\rho c_p$.

The steady-state solution for $\theta_{l,ml}$, as derived in section can be rewritten:

$$\theta_{l,ml} = \frac{C_d|\vec{U}|\theta_{l,0} + w_e\theta_{l,fa}|_{z=z_i} - F'}{C_d|\vec{U}| + w_e} = \frac{\theta_{l,0} + w_e(\theta_{fa}|_{z=z_i} - \theta_0) - F'}{C_d|\vec{U}| + w_e}. \tag{A.2}$$

With this thesis' implementation $\psi_{fa} = \psi_{ref} + \delta\psi + \Gamma_\psi$, where ψ_{ref} is a reference value evaluated at $288K$, $\theta_{l,fa}$ can be written:

$$\theta_{l,fa}(z) = \theta_{ref} + \delta\theta + \Gamma_\theta z. \tag{A.3}$$

Together with the equation for the entrainment in steady-state,

$$w_e = Dz_i, \tag{A.4}$$

these equations together make way to find a solution for $\theta_{l,ml}$, z_i, w_e and eventually $q_{t,ml}$.

Substituting the entrainment out of equations (A.1) and (A.2) by using (A.4) one finds:

$$\theta_{l,ml} = \theta_{l,0} + \frac{Dz_i(\theta_{fa}|_{z=z_i} - \theta_{l,0}) - F'/\rho c_p}{C_d|\vec{U}| + Dz_i} \tag{A.5}$$

$$Dz_i\Delta\theta_l = AF'. \tag{A.6}$$

Combining both these equations yields:

$$Dz_i\left[\theta_{fa}|_{z=z_i} - \theta_{l,0} - \frac{Dz_i(\theta_{fa}|_{z=z_i} - \theta_{l,0}) - F'}{C_d|\vec{U}| + Dz_i}\right] - AF' = 0, \tag{A.7}$$

which can be rewritten:

$$Dz_i\left[(C_d|\vec{U}| + Dz_i)(\theta_{fa}|_{z=z_i} - \theta_{l,0}) - Dz_i(\theta_{fa}|_{z=z_i} - \theta_{l,0}) + dF_L\right] - AF'(C_d|\vec{U}| + Dz_i) = Dz_iC_d|\vec{U}|(\theta_{fa}|_{z=z_i} - \theta_{l,0}) - F'\left[AC_d|\vec{U}| + Dz_i(A-1)\right] \tag{A.8}$$

Now substituting in $\theta_{l,fa}|_{z=z_i} = \theta_{ref} + \delta\theta + \Gamma_\theta z_i$ the equation will only be dependent on unknown z_i:

$$Dz_i C_d|\vec{U}|(\theta_{ref} - \theta_{l,0} + \delta\theta + \Gamma_\theta z_i) - F'\left[AC_d|\vec{U}| + Dz_i(A-1)\right] = 0, \quad \text{(A.9)}$$

or in familiar fashion

$$z_i^2 + z_i\left[\frac{C_d|\vec{U}|(\theta_{ref} - \theta_{l,0} + \delta\theta) + (1-A)F'}{C_d|\vec{U}|\Gamma_\theta}\right] - \frac{AF'}{D\Gamma_\theta} = 0. \quad \text{(A.10)}$$

This can easily be solved to gain an expression for z_i :

$$\begin{array}{c} z_i = \frac{1}{2\Gamma_\theta}\left[\frac{(A-1)F'}{C_d|\vec{U}|} - \theta_{ref} + \theta_{l,0} - \delta\theta\right] \\ + \frac{1}{2\Gamma_\theta}\sqrt{\left(\frac{(A-1)F'}{C_d|\vec{U}|} - \theta_{ref} + \theta_{l,0} - \delta\theta\right)^2 + \frac{4AF'\Gamma_\theta}{D}} \end{array} \quad \text{(A.11)}$$

The solutions of $\theta_{l,ml}$, z_i and w_e can now be completed with the solution for $q_{t,ml}$ that just depends on z_i when equation (A.4) and

$$q_{t,fa}(z) = q_{ref} + \delta q_t + \Gamma_q z \quad \text{(A.12)}$$

are inserted in equation (2.37):

$$q_{t,ml} = \frac{C_d|\vec{U}|q_{t,0} + w_e q_{t,fa}|_{z=z_i}}{C_d|\vec{U}| + w_e} \quad \text{(A.13)}$$

z_i can now be differentiated with respect to $\theta_{l,0}$:

$$\frac{\partial z_i}{\partial\theta_{l,0}} = \frac{1}{2\Gamma_\theta}\left(\frac{\theta_{l,0} - \theta_{ref} - \delta\theta + \frac{(A-1)dF_L}{C_d|\vec{U}|}}{\sqrt{(\theta_{l,0} - \theta_{ref} - \delta\theta + \frac{(A-1)dF_L}{C_d|\vec{U}|})^2 + \frac{4AdF_L\Gamma_\theta}{D}}} + 1\right). \quad \text{(A.14)}$$

Bibliography

[1] S. Bony, R. Colman, Vladimir M. Kattsov et al. How well do we understand and evaluate climate change feedback processes. *Journal of Climate*, 19, 2006.

[2] J.W.M. Cuijpers. *Large-Eddy Simulation of Cumulus Convection*. PhD thesis, TUDelft, 1994.

[3] D.A. Bennetts, E. McCallum and S. Nicholls. Stratocumulus: an introductory account. *The Meteorological Magazine*, 115, 1986.

[4] W.H. Schubert et al. Marine stratocumulus convection: Part I: Governing equations and horizontally homogeneous solutions. *Journal of the Atmospheric Sciences*, 36, 1979.

[5] D.K. Lilly. Models of cloud-topped mixed layers under a strong inversion. *The Quarterly Journal of the Royal Meteorological Society*, 94:292–309, 1968.

[6] B. Stevens. Entrainment in stratocumulus-topped mixed layers. 2002.

[7] CGILS. $http://atmgcm.msrc.sunysb.edu/cfmip\_figs/case\_specification.html$.

[8] R.B. Stull. *An Introduction to Boundary Layer Meteorology*. 1986.

[9] S.R. de Roode. *Clouds*. University of Utrecht, 2004.

[10] B. Stevens. Cloud transitions and decoupling in shear-free stratocumulus-topped boundary layers. *Geophysical Research Letters*, 27:2557–2560, 2000.

[11] J.J. van der Dussen. Large Eddy and Mixed-Layer Model Simulation of the Stratocumulus to Cumulus Transition as Observed During ASTEX. Master's thesis, Delft University of Technology, 2009.

[12] C.-H. Moeng. Entrainment rate, cloud fraction and liquid water path of planetary boundary layer stratocumulus clouds. *Journal of the Atmospheric Sciences*, 57:3627–3643, 2000.

[13] S.R. de Roode, G. Lenderink and M. Koehler. The representation of entrainment in stratocumulus-topped boundary layers with a TKE model.

[14] B. Stevens. Bulk boundary-layer concepts for simplified models of tropical dynamics. 2006.

[15] D. Johnson, W.H. Schubert, B.A. Albrecht, C.S. Bretherton and A.S. Frisch. The atlantic stratocumulus transition experiment - ASTEX. *Bulletin of the American Meteorological Society*, 76.

[16] T. Heus et al. Formulation of and numerical studies with the Dutch Atmospheric Large-Eddy Simulation (DALES). *Geoscientific Model Development Discussions*, 2010.